Paulo Edgar Geraldes Fernandes

Bachelor of Science in Micro and Nanotechnologies Engineering

Fabrication of Skin-Like Sensors in Thin Polymeric Membranes

Dissertation submitted in partial fulfillment
of the requirements for the degree of

Master of Science in
Micro and Nanotechnologies Engineering

Adviser: Rui Alberto Garção Barreira do Nascimento Igreja, Associate Professor, Faculty of Sciences and Technology NOVA University of Lisbon

Co-adviser: Joana Vaz Pinto, Assistant Professor, Faculty of Sciences and Technology NOVA University of Lisbon

Examination Committee

Chairperson: Prof. Dr. Luís Miguel Nunes Pereira
Raporteur: Prof. Dr. Hugo Manuel Brito Águas
Member: Prof. Dr. Rui Alberto Garção Barreira do Nascimento Igreja

FACULDADE DE
CIÊNCIAS E TECNOLOGIA
UNIVERSIDADE NOVA DE LISBOA

October, 2019

Fabrication of Skin-Like Sensors in Thin Polymeric Membranes

This document was created using the (pdf)LaTeX processor, based in the "novathesis" template[1], developed at the Dep. Informática of FCT-NOVA [2].
[1] https://github.com/joaomlourenco/novathesis [2] http://www.di.fct.unl.pt

"O mundo em si não tem sentido sem o nosso olhar que lhe atribui identidade, sem o nosso pensamento que lhe confere alguma ordem."

- Lya Luft

Acknowledgements

No final deste longo ciclo, muitos são os agradecimentos que gostaria de fazer a tantas pessoas que contribuíram para a minha formação académica e crescimento como Homem. Gostaria de começar por agradecer à Faculdade de Ciências e Tecnologia da Universidade Nova de Lisboa pela minha formação, nomeadamente a Professora Dra. Elvira Fortunato e Professor Dr. Rodrigo Martins pela criação e desenvolvimento do curso de Engenharia de Micro e Nanotecnologias e pelas condições de trabalho oferecidas no CENIMAT|i3N e CEMOP.

Queria agradecer ao meu orientador, professor Rui Igreja pela orientação e ajuda no desenvolvimento desta tese e deixar também um agradecimento especial à minha co-orientadora professora Joana Vaz Pinto, pela apoio, paciência e motivação que me deu desde o primeiro dia.

Um muito obrigado à Andreia dos Santos por toda a ajuda que me deu durante esta dissertação.

Se existe alguém que não posso esquecer, por toda a ajuda e amizade durante este meu percurso, essa pessoa é o Bernardo de Melo, muito obrigado por tudo.

À Ana Teresa Pimentel por toda a dedicação e paciência que teve comigo nos meus primeiros anos de faculdade, à Jenny Boane por toda ajuda no processo de Langmuir-Blodgett, ao Ricardo Ribeiro e ao Tomás Freire por toda o apoio que me deram na escrita e elaboração da tese e ao João Barrulas pela "formação" em LaTeX. Bem como a toda a equipa do CENIMAT que sempre se mostraram prestáveis e prontos a ajudar.

À anTUNiA a todos os membros sem exceção, pois grande parte do que sou hoje devo a esta instituição, obrigado por toda a ajuda e motivação para nunca desistir.

À minha minha família em especial à minha irmã Diana Fernandes por todo o apoio que me deu e pela motivação que me transmitiu nas horas mais difíceis, e finalmente dedicar tudo isto aos meus pais, pois sem o apoio deles seguramente não teria sido possível eu chegar aqui.

Abstract

Recently, research in health care improved the creation of devices that accurately monitor various physiological stimuli (wearable devices) which provide better health care and help to predict possible diseases through continuous data collection. However, wearable devices are at an early stage of development and several improvements must be made, both at structural and materials level. Some examples of devices on the market such as smartwatches or fitness bands are still very bulky and the goal is to make them as small and functional as possible.

This work focuses on the improvement of fabrication process steps of pressure sensors, based on micro-structured thin polymeric films of Polydimethylsiloxane (PDMS) or Parylene C, namely micro-structuration techniques and electrode deposition. To create dome-shaped structures, Polystyrene (PS) microspheres were deposited by Langmuir-Blodgett (LB) process over Parylene C and then subjected to a Reactive Ion Etching (RIE) process to create the mold. Pyramidal structures were made by anisotropic etching of silicon with potassium hydroxide (KOH) to make molds. Both molds were further used to produce micro-structured PDMS films by soft lithography. Through these techniques, PDMS domes with diameters between 2.3 μm and 3.0 μm and heights between 1.6 μm and 1.7 μm, and PDMS pyramids with a size of 50 μm to 100 μm and a height of 34.3 μm to 66.4 μm were achieved.

To work as a piezoresistive pressure sensor, the micro-structures must be covered with a conductive layer that will play the role of electrode. To overcome adhesion issues between PDMS and some metals, the possibility of using a thin film of Parylene C on top of PDMS was studied. The metals explored were aluminium, copper, and titanium with gold, where the latter presented better adhesion and electrical properties.

The developed micro-structured films were assembled and tested as piezoresistive or capacitive pressure sensors achieving sensitivities up to -1.1×10^{-2} kPa^{-1} and 3.1×10^{-2} kPa^{-1} respectively.

Keywords: Wearable devices; PDMS; Parylene C; Pressure sensors; Metals adhesion.

Resumo

Estudos realizados para a melhoria da saúde levaram à criação de dispositivos que meçam sinais fisiológicos com precisão e que possam ser adaptados ao corpo humano ou ao vestuário (dispositivos *wearables*), fornecendo melhores cuidados de saúde e ajudando na prevenção de possíveis doenças através da recolha contínua de dados. No entanto, este tipo de dispositivos *wearables* encontram-se ainda num estado inicial de desenvolvimento e várias melhorias podem ainda ser feitas, tanto a nível estrutural quanto de materiais. Alguns exemplos de dispositivos no mercado, como *smartwatches* ou *fitness bands*, ainda são muito volumosos e o objetivo é torná-los o mais pequenos e funcionais possível.

Este trabalho foca-se na melhoria das etapas do processo de fabricação de sensores de pressão, baseados em filmes poliméricos finos micro-estruturados de polidimetilsiloxano (PDMS) ou Parileno C, nomeadamente técnicas de microestruturação e deposição de eletrodos. De modo a criar estruturas em forma de cúpula, microesfera de poliestireno (PS) foram depositadas pelo processo de Langmuir-Blodgett (LB) sobre Parileno C e depois submetidas a um processo de erosão por *Reactive Ion Etching* (RIE) para criar o molde. As estruturas piramidais foram feitas por erosão anisotrópica de silício com hidróxido de potássio (KOH) para fazer moldes. Ambos os moldes foram utilizados para produzir filmes microestruturados de PDMS. Através destas técnicas, cúpulas de PDMS com diâmetros entre 2,3 μm e 3,0 μm e alturas entre 1,6 μm e 1,7 μm, e pirâmides de PDMS com tamanho de 50 μm a 100 μm e altura de 34,3 μm a 66,4 μm foram obtidas.

Para funcionar como um sensor de pressão piezoresistivo, as microestruturas devem ser cobertas com uma camada condutora que desempenhará o papel de elétrodo. De modo a superar os problemas de adesão entre o PDMS e alguns metais, estudou-se a possibilidade de usar uma película fina de Parileno C em cima do PDMS. Os metais explorados foram alumínio, cobre, e titânio com ouro, sendo que estes últimos apresentaram melhor aderência e propriedades elétricas.

Os filmes microestruturados desenvolvidos foram montados e testados como sensores de pressão piezoresistivos ou capacitivos sendo possível alcançar sensibilidades de -1.1×10^{-2} kPa^{-1} e 3.1×10^{-2} kPa^{-1} respectivamente.

Palavras-chave: Despositivos vestíveis; PDMS; Parileno C; Sensores de pressão; Adesão de metais.

Contents

List of Figures

List of Tables

Acronyms

AFM	Atomic Force Microscopy.
CVD	Chemical Vapor Deposition.
ECG	Electrocardiogram.
IPA	Isopropyl Alcohol.
LB	Langmuir-Blodgett.
LD	large dome.
LP	large pyramid.
PDMS	Polydimethylsiloxane.
PET	Polyethylene Terephthalate.
PS	Polystyrene.
RIE	Reactive Ion Etching.
SCCM	Standard Cubic Centimeters per Minute.
SD	small dome.
SEM	Scanning Electron Microscopy.
SP	small pyramid.

Objectives and Motivation

The ever-growing demand for wearable devices has lead research into making them smaller and more functional, not only looking for new materials for their construction, but also improving existing ones [7, 22].

PDMS is the most used material in wearable devices due to its biocompatibility, elasticity, flexibility, etc. However, despite having some similarities with the human skin, this material has some drawbacks, such as high relaxation time, low surface energy, and incompatibility with etching processes [17, 31]. The solution to overcoming the relaxation time problem is to create microstructured PDMS films[25, 31]. Since PDMS is not easy to structure by etching methods, it is necessary to resort to the use of mold structuring which has led to a demand for innovation in the creation of new and better molds[1, 22].

Owing to the insulating nature of elastomers like PDMS it is necessary to apply a layer of metal adhesion to act as an electrode in the final device [7]. This becomes a problem due to the PDMS low surface energy which makes it difficult for the metal to stick on its surface [12]. Plasma treatments are reported in the literature as a solution to improve adhesion, however this area requires further investigation [4, 17].

The main purpose of this dissertation was the study new processes to create molds, like using Parylene C or Acrylic as a substrate to deposit a PS microspheres layer by LB process or pyramidal structures etched on Silicon, as well as to study metal adhesion on PDMS and produce capacitive and piezoresisteve pressure sensors.

Chapter 1

Introduction

1.1 Wearable devices

The rapid growth and development in consumer technology has been accompanied by an increase in the availability to the general population. That is true for smart electronics (smartwatches, smart bands) that are now widely available bringing with them a plethora of advantages, allowing for personal monitoring of medical parameters anywhere and in real time such as heart rate, calorie loss, body temperature, etc.

Electronic skins, commonly known as E-skins, have the goal of artificially recreating human skin [7, 22]. To create E-skins many difficult challenges appear at the beginning, given that human skin has a high flexibility and stretchability as well as the ability to detect pressure, temperature, shear, humidity, mechanical forces, fluid flow, pain and so on [4, 19]. However, this field has taken the first steps and has made incredible advances in recent years, creating a bridge between man and machine, thus enabling a more personalized and on the fly health monitoring [10, 22].

The principle of operation is based on converting physiological signals into electrical signals, collection data by continuous measurement of signals such as pulse, temperature and electrocardiogram (ECG), as well as the possibility to save these data [13]. Due to the wide range of applications that can be applied to a wearable device, there are different types of devices with different shapes, sizes and compositions, and the way they work depends on their purpose and where they will be applied [33]. Through the continuous data collection of physiological and electrophysiological activity responses, it is possible to study their clinical relevance for diseases such as heart failure, epilepsy and Parkinson [29].

The great application potential of this technology extends not only to health monitoring but also to areas such as intelligent robots, biomimetic prostheses or drug delivery. However, this technology is still in an early stage of development [22, 33]. Figure 1.1 shows some of the possible applications for a wearable device, as well as the different types of sensors that can monitor physiological activity.

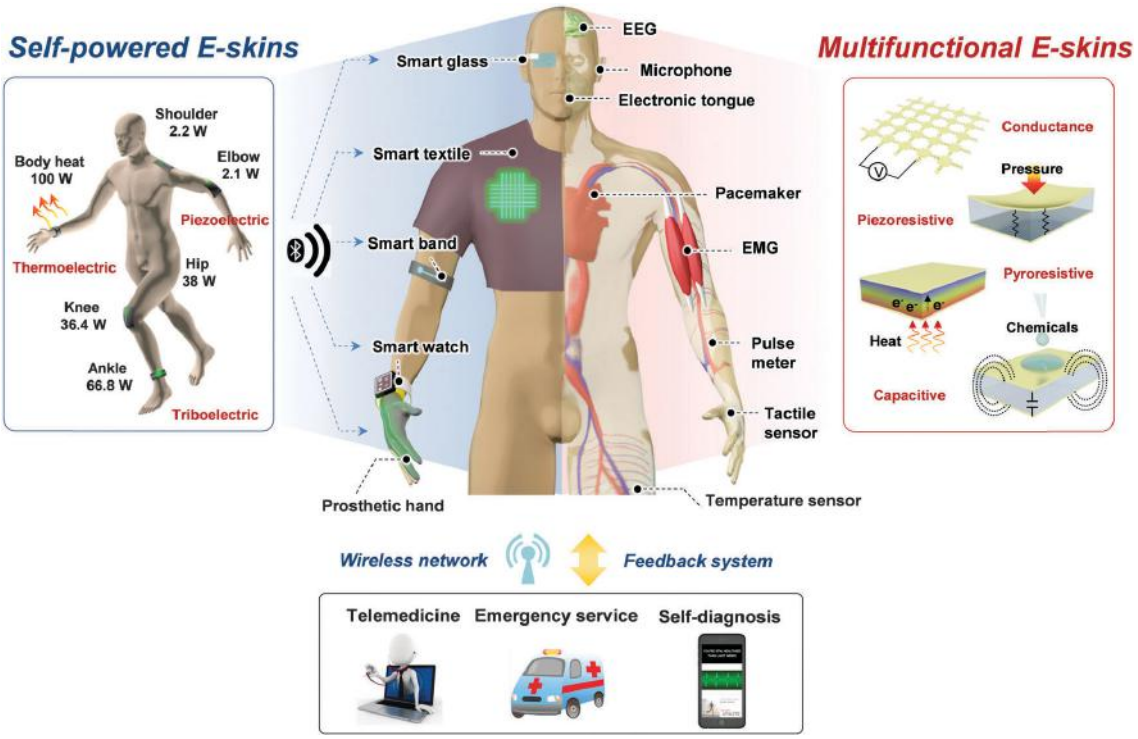

Figure 1.1: Types of wearable devices and their applications [22].

1.2 Pressure sensors

In order to create a pressure sensor that becomes a wearable device, several aspects should be considered, such as mechanical properties, flexibility and especially the high sensitivity capable of operating in a low pressure (<10 kPa) regime [2, 7]. The growing demand for these devices and their versatility increases the need to customize the sensors in order to adapt to the required needs. However, in their production it is necessary to consider factors that affect their performance, like planning their design to achieve the desired performance, and choosing the materials to create the dielectric layer and the electrodes [33].

Usually, dielectrics are made from elastomeric materials, such as Polydimethylsiloxane (PDMS), because of their high elasticity and compressibility that allow them to control the sensor sensitivity and working range by micro-structuring these materials [10, 15]. The electrodes are usually metals, but several studies have been done using nanomaterials, such as silver nanowires or carbon nanotubes [14, 20].

There are several types of pressure sensors that can be classified, based on their operating mode, as capacitive [27], piezoresistive [4, 6], piezoelectric [3] or triboelectric [5].

Capacitive sensors work by converting mechanical stress into a capacitance (C) change [22]. When applying pressure, the elastomeric dielectric layer is deformed inducing a change in the capacitance of the sensor, as shown in Figure 1.2(a). These sensors are

projected through equation 1.1 where ϵ_r is the dielectric constant, ϵ_0 is the vacuum permittivity, A is the electrode area and d is the distance between two electrodes.

$$C = \frac{\epsilon_r \epsilon_0 A}{d} \tag{1.1}$$

The possibility to modify the geometry by changing the variables A and d confers a great versatility to this sensor, allowing it to be used in a wide range of applications [22]. This type of sensors requires low power consumption and is usually used to measure static forces with a high pressure sensitivity and mechanical flexibility [22, 25].

Piezoresistive sensors are the most widely used in wearables [22]. They recognize the stimuli by electrical resistance changes, which can be done by band-structure changes in semiconductors [34], variation in contact resistance between conducting materials [20], and alternation of conductive networks under mechanical deformations [23]. Piezoresistive sensors have a simple structure and operation mode, although they are sensitive to the temperature and require constant power supply [25]. They have high elasticity and can be combined with other sensors (temperature, light, flow, ECG sensors, etc.) [22]. When pressure is applied on two patterned layers with the structures facing each other like a sandwich, the contact area between the structures varies, giving rise to a resistance change, as shown in Figure 1.2(b) [19]. This strategy conferes a high pressure sensitivity to this type of sensors.

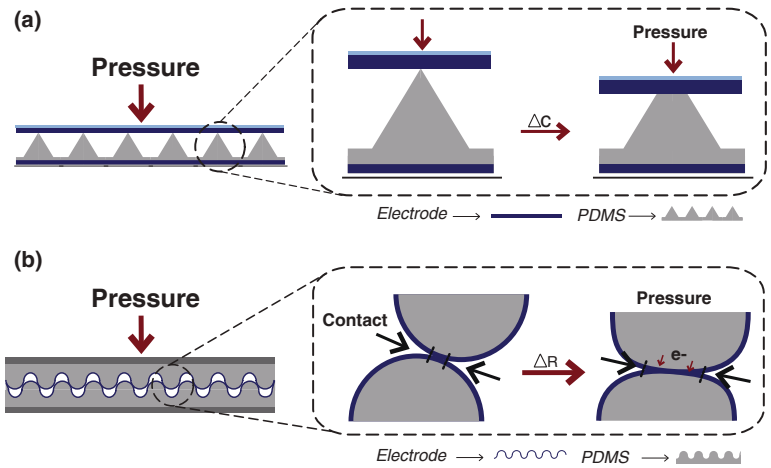

Figure 1.2: Pressure sensor schematics. (a) Example of a capacitive sensor with pyramid-shaped microstructures, this structure can also work as a piezoresistive sensor; (b) Piezoresistive sensor with dome-shaped structures.

Piezoelectric sensors work through the ability of certain materials to generate electrical charges by mechanical stress [3], while triboelectric sensors work based on the

triboelectric phenomenon commonly known as static electricity [5]. In one hand, these sensors have a fast response rate to dynamic stimuli, which gives them a limitation when the external stimulus is static. In the other hand, capacitive and piezoresistive sensors detect, with high accuracy, several stimuli such as pressure, temperature, chemical stimuli or humidity, as well as detect forces applied in different directions, thus enabling the device to perform a continuous monitoring [22].

1.3 PDSM and Parylene C

PDMS is an elastomeric silicone material that due to its intrinsic properties became the main choice for flexible electronics substrate such as e-skins [31]. Among these properties one can highlight the good biocompatibility, elasticity, flexibility, lack of toxicity, chemical inertness, thermal stability, as well as the fact that it is a transparent material, cheap and of easy processing [1, 12, 17]. There are, however, some limitations associated with PDMS such as its viscoelastic properties that are responsible for an increase of relaxation times of PDMS-based devices upon pressure [19, 33]. Due to the insulating nature of PDMS the conductivity will have to be achieved by introducing a conductive material, like metal, but the PDMS low surface energy often causes difficulties in metal adhesion, and even when a metal is successfully deposited, it can be easily damaged or debonded [12].

Poly(para-xylylenes), usually known by parylene, is a semi-crystalline thermoplastic polymer that was discovered in 1947 by polymerization of p-xylene [16]. This polymer can be described by a linear chain benzene ring wherein two methylene groups replace two hydrogen atoms that serve as coupling links. More than 20 parylene derivatives are known, which can be identified by molecules that replace hydrogen atoms [24]. The most used type of parylene, for its cost and properties (light, flexible, mechanically strong and optically transparent) is Parylene C which has a chlorine atom on the benzene ring [8]. This polymer has interesting features for integration in wearables, given that it is biocompatible, biostable, has good dielectric properties, low permeability, and does not react with most chemicals, but have the main disadvantage of low fatigue wear resistance property [11, 24]. The method to create this polymer was improved over the years by pyrolysis of the dimer form of the material, and today, a steam deposition process is used, which allows a deposition capable of covering any geometry with a uniform and consistent thickness [16].

In the Table 1.1 are presented, for both materials, the main electric and mechanical constants which need to be attended in order to produce the device.

1.4 Microstructured surfaces

The research for improvement and adaptability of wearable devices involves not only the study of new materials but also the study of structures that can improve their performance. PDMS has a significant hysteresis and long relaxation time that result from

Table 1.1: Properties of parylene C and PDMS [24]

Property	Parylene C	PDMS
Dielectric Constant (1 kHz)	3.10	2.3 – 2.8
Young's Modulus (Pa)	2.76×10^{9}	3.59×10^{5} – 8.69×10^{5}
Elongation to Break (%)	200	210 – 310

their viscoelastic nature and can be minimized through micro-structuration improving the sensors' sensitivity and relaxation time [10, 15, 25].

Various designs for structured films have been studied, based on biostructures such as epidermal-dermal microstructures of the human skin [21], plant surfaces or insect wings [18, 28], textile materials like silk [31], or engineered 3D structures like pyramids [25], cones [26], cubes [5], wrinkles [32], dome-shaped surfaces [19] or porous structures [9]. In order to create these films, a mold has to be constructed. Usually, a rigid material such as silicon or acrylic is used, but PDMS has also been reported as a mold [4, 5].

The most popular way to create molds is by photolithography processes, which although expensive and complex processes which, despite being expensive and complex, provide molds with a good definition [25].

CHAPTER 2

MATERIALS AND METHODS

2.1 PDMS and Parylene C films

Two different substrates (silicon and glass) were used along this work as carriers to produce microstructured membranes. Before any processing these substrates were cleaned using an ultrasound bath, in acetone, Isopropyl Alcohol (IPA) and deionized water, sequentially.

Parylene C thin films were produced by chemical vapor deposition (CVD) using a Specialty Coating System Model *PDS 2010 Labcoter 2*. The parylen film thickness is controlled by the amount of Parylene dimer loaded on the system, that in this work was set to 5 - 10 g in order to produce membranes with an average thickness between 3 to 7 μm.

PDMS films were prepared by mixing silicone elastomer and curing agent (Sylgar 184) in a volume ratio of 10:1. After stirring, the mixture is degassed for several minutes to remove all the air bubbles created by the mixing process. These films are produced by spin coating the PDMS mixture. In this process the angular velocity controls the final thickness of the membranes and it was varied between 200 rpm and 1900 rpm with a constant acceleration of 100 rpm/s. The PDMS films are then cured at 80 °C for 1 hour.

2.2 Production of micro-structured molds for PDMS films

Two different approaches were explored in this work to produce molds for PDMS micro structuring: the use of polystyrene microspheres as a physical mask dispersed by Langmuir-Blodgett and subsequent reactive ion etching processes (subsection 2.3.1) and anisotropic wet-etching of silicon in KOH solution to produce inverted pyramids in silicon (subsection 2.3.1).

2.2.1 Langmuir-Blodgett Deposition Method and Reactive Ion Etching (RIE)

Langmuir Blodgett techniques was performed in a *KSV NIMA LangmuirBlodgett Medium Deposition*, and the deposited material were polystyrene ($(C_8H_8)n$) microspheres with an average diameter of 4.98 μm from microParticles GmbH. 200 μL of PS microspheres were

dispersed in ethanol and centrifuged 4 times at 3300 rpm in a REMI16 centrifuge. The microspheres were then left in an ethanol suspension for 12 hours and finally sonicated with pure ethanol. The substrates to be cover (in this particular case silicon coated with Parylene C) are placed in the equipment's sample holder and dipped in the trough of the equipment, and the microspheres suspension is slowly loaded on the water surface with a syringe. Seting an initial surface tension of 18 mN/m, the substrates are then slowly pulled out of the water at a speed of 2 mm/min, as shown in Figure B.1.

This monolayer of PS microspheres will be used as a physical mask in a reactive Ion Etching [30] system in a *Trion Minilock Phantom III*, Figure B.2. The samples used in this process were Si/Parylene C covered with PS-microspheres, and were patterened using an oxygen plasma with the following parameters: O_2 gas flow of 10 sccm, power of 50 W, and a process pressure of 6 Pa. The oxygen plasma etches both unmasked regions of Parylene membrane and the PS microspheres so that the final structure consists in elevations or cavities spread along the etched area.

Negative replica of this patterned Parylene C was made by covering it with silicone elastomer and curing agent (Sylgard 184), previously mixed in a volume ratio of 5:1, and degassed for 30 min to remove air bubbles and increase the fidelity of the pattern negative replica. Then, the PDMS mixture was cured at 80 °C for one hour, and peeled off from the patterned Parylene C.

2.2.2 Anisotropic wet-etching

Anisotropic wet-etching of silicon was performed with potassium hydroxide etching solution (KOH) prepared with 40% concentration. Silicon wafers coated with 100 nm of thermal oxide SiO_2 and silicon wafers coated with 145 nm of Si_3N_4 films were used as a mask to protect against etching is specific regions of the wafers, while unmasked Si regions are etched. Photolitography masks were designed and produced with two patterns: squares of 100 μm and and squares 50 μm squares. These patterns were transferred by photolithography to SiO_2 and Si_3N_4 films and the molds were produced by etching Si in KOH anisotropic bath at 80 ºC for the required time to insure a full inverted pyramid formation on silicon.

2.3 Production of micro-structured PDMS films

PDMS films were prepared by mixing silicone elastomer and curing agent s mentioned preciously. The mixture was spin-coated on the produced molds with a spinning time of 90 seconds at 250 rpm and an with acceleration of 100 rpm/s. Finally, the PDMS films were cured at 80 °C for one hour and peeled off from the molds. The molds (either microstructred denser PDMS or Si based inverted pyramids) were subjected to a silanization process before PDMS spin-coating to facilitate the peel-off of the membranes.

2.4 Metal deposition

Different metals were deposited during this work using either an electron-beam assisted evaporation system (E-beam) or a resistive thermal evaporation. Ti/Au (6 nm / 60 nm), Cu (150 nm), and Al (100 nm) films were deposited in home made e-beam evaporation system in CEMOP Clean room, insuring a base pressure (before deposition) below 6×10^{-6} mbar and growth rates between 0.5 to 3 nm/s. Thermal evaporation was also performed to deposit aluminium films in a Home-made system located at Lab2 of CENIMAT. All depositions were performed at a base pressure of 3×10^{-6} mBar or lower insuring a high mean free path and to guarantee that no oxidation occurs during the process. Aluminium films with a thickness of 75 nm produced as an alternative to E-beam deposition.

2.5 Production of pressure sensors

Two types of sensors (piezoresistive and capacitive) were produced. In the piezoresistive sensors, two microstructured films coated with Ti/Au (electrode) were assembled facing each other like a sandwich. Two copper wires were glued with silver glue to each electrode so that the sensor could be mounted on a circuit for sensitivity measurements. In capacitive sensors, the electrode Ti/Au was deposited on the unstructured side of the PDMS films. A single microstructured film was sandwiched with PET/ITO. Two copper wires were glued with silver glue to the electrodes for further measurements.

2.6 Characterization

Thickness measurements were performed using, a *Ambios XPprofilometer* equipped with 2 μm radius stylus. The morphology of the microstructures produced was verified through a *Hitachi TM 3030Plus Tabletop* scanning electron microscope (SEM). The electrical characterization in the piezoresistive sensors was made by applying 5 V to the sensor, and measuring the signal upon pressure (0.27 kPa and 30.3 kPa) with an oscilloscope. In the capacitive sensors different pressures between 0 and 4.28 kPa were applied to the device to measure its capacitance. A Lock-In Amplifier (*ModelSR830*) was connected to both contacts of the sensor to measure the current module while applying a voltage of 0.1 V at 5000 Hz frequency.

CHAPTER 3

RESULTS AND DISCUSSION

3.1 Membrane Production

For e-skin like sensors it is important to guarantee their flexibility, which implies that the films composing the sensor are thin enough. Therefore, the thickness variation of PDMS films and Parylene C films was studied by changing the spinner rotation speed or the amount of parylene dimer, respectively. Additionally, the peel-off of these films from their respective substrates (glass or silicon wafer) or molds was studied.

3.1.1 PDMS Thickness

The PDMS films' thickness was studied by varying the spinner rotation speed between 200 rpm and 1900 rpm, while keeping all other spin-coating parameters constant. Figure 3.1 shows the results of this test, highlighting that it is possible to reach a PDMS film thickness of only 17 μm with a spinner rotation speed of 1900 rpm.

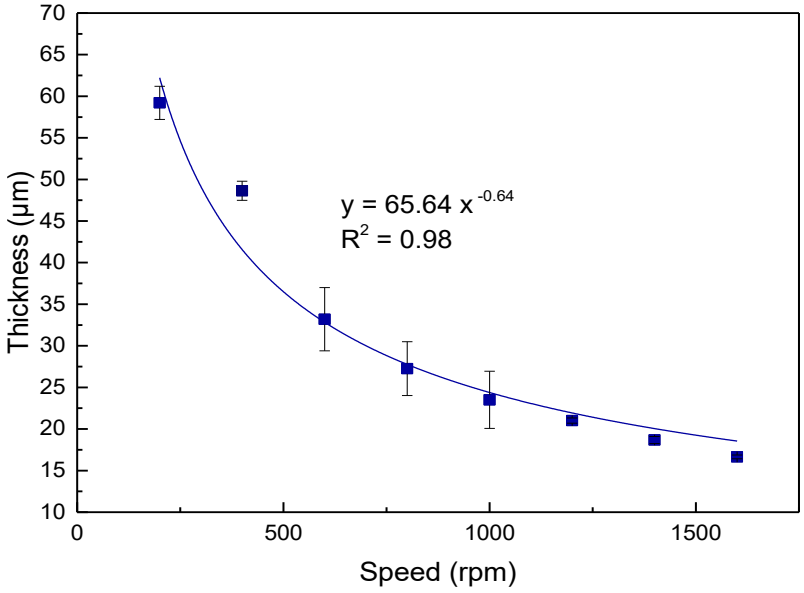

Figure 3.1: PDMS thickness varying with spinner rotation speed.

3.1.2 Parylene C Thickness

The Parylene C thickness can be controlled through the dimmer mass that is loaded into the vaporization chamber. Figure 3.2 shows the results for this test, made with 9 different dimmer masses, where it is possible to conclude that the Parylene C thickness can be controlled with high precision and in a linear way with the dimmer mass, with a linear regression of y = ax + b, where y is the thickness of the film in μm, and x is the dimmer mass in g.

Studies show that if a substrate that was previos coated with PVA, the paryline C peel-off can be easily made [16], that makes him an interesting material to be studied in the future as PDMS microstructured filme alternative.

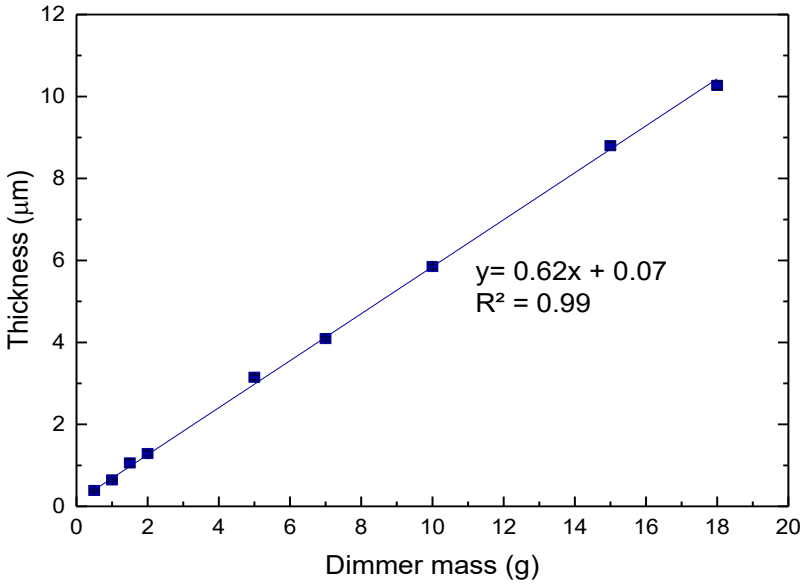

Figure 3.2: Parylene C thickness test varying the dimmer mass.

Since in this work Parylene C was mainly used as a substrate for mold production, its thickness was kept constant above 6 μm, since most of Parylne C depositions were performed with 10 g dimer weight.

3.1.3 Peel-Off

PDMS peel-off is easily done if the substrate or mold surface was previous silanized or covered with PVA. How easily this process is done depends not only on the skill of the operator but also on the thickness of PDMS. When a substrate is silanized, the peel-off is simple and only requires tweezers to pull the film and a scalpel to help peeling-off the edges of the film. The thinner the film is, the more complicated the process becomes, not only because of the risk of tearing the film upon pulling, but also because the film tends to curl when it loses contact with the substrate due to static electricity. In order to study the peel-off difficulty with PDMS thickness, PDMS films with different thicknesses,

controlled by the spinner rotation speed, were peeled-off from silanized glasses. For each sample, the difficulty in the peel-off process was evaluated.

As shown in the Table 3.1, PDMS films with thicknesses down to 48.6 μm do not tend to curl after the peel-off. For films with a thickness below 21 μm, they immediately curl after the peel-off, which makes it very hard to work with such films, Figure 3.3.

Table 3.1: Observations regarding the difficulty in the peel-off process of PDMS films with different thicknesses.

Rotation (rpm)	**Thickness** (μm)	**Filme**
200	59.2	Does not Curl
400	48.6	Does not Curl
600	33.2	Tends to Curl
800	27.1	Tends to Curl
1000	23.5	Tends to Curl
1200	21.0	Curls
1400	18.7	Curls
1600	16.6	Curls

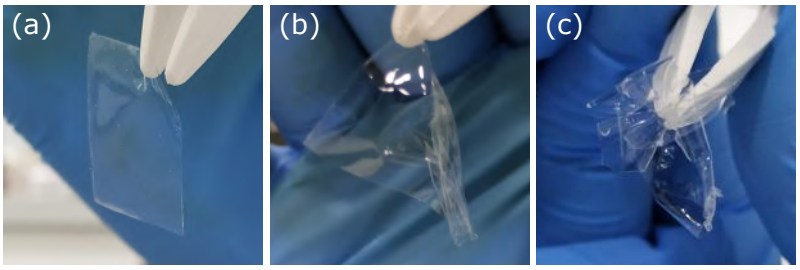

Figure 3.3: Examples of PDMS films after peel off (a) PDMS film not curled; (b) PDMS film tending to curl; (c) PDMS film curled.

For intermediary thicknesses, the films show some tendency to curl. Instead of subjecting the substrates to a silanization process, a PVA coating was explored to help in the peel-off process. Despite being a longer process than silanization, this strategy avoids the tendency of the PDMS films to curl after being detached from the substrate because the substrate is submerged in water to dissolve the PVA layer. Nevertheless, when one tries to remove the PDMS films from the water, they also tend to curl, which can be solved if both substrate and film are removed from the water at the same time.

3.2 Metal adhesion to PDMS or Parylene C filmes

One of the most important issues in the metal adhesion to a polymeric substrate is that the adhesion has to be strong enough so that the metal will not easily peel-off from the polymeric film after deposition or suffer any damage. Given the well-known issues regarding the adhesion of metals to PDMS films, some surface treatments, such as oxygen

plasma treatment, have been suggested in the literature to improve the bond between these two materials [1, 12].

In order to find an alternative to improve the metal adhesion to the PDMS, Parylene C was studied as an adhesion layer for PDMS, and proved to be successful as shown in Appendix A. Additionally, it was found that actually some metals can be deposited on PDMS without any treatment. The selected metal for this adhesion study were copper (Cu), titanium and gold (Ti/Au), and aluminum (Al), with the latter being deposited by thermal evaporation while the other metals were deposited by E-beam. These metals were deposited over plain PDMS films, PDMS films covered with parylene C, and glass as a control for the deposition process, achieving a metal thickness of 6/60 nm for Ti/Au and 150 nm for Cu. For the Al it was achieved the thicknesses of 75 nm in the thermal evaporation technique and 100 nm in the E-beam.

In Appendix A (Figures A.1, A.2, and A.3) it is possible to see an image of each sample, and as shown in Figure A.1 for Al, all depositions were well achieved and presented a good adhesion to the substrate, with the exception of Al deposited on PDMS by thermal evaporation. This sample did not show a shiny appearance, a possible explenation is that PDMS is a porous material and the vacuum made in the thermal evaporation system chamber was not high enough to remove all oxygen in the pores of the PDMS. The oxygen that remains in the pores reacts with the evaporated aluminum by oxidizing it, causing the Al deposition in the PDMS not to be successful, Figure 3.4. To clarify this issue, Al was deposited on PDMS by E-beam in higher vacuum conditions (than those used in the evaporator), and as it is possible to see in Figure 3.4, the deposition was well achieved.

The electrical characterization of the metal layer was made through the analysis of its sheet resistance (R_S). To determine the R_S a rectangular area of the metal layer was defined with conductive copper tape as shown in Figure 3.4, with L representing the distance between the two copper tapes and W representing the length of the copper tape that is in contact with the metallic film.

Using a multimeter to measure the resistance (R) between both copper tapes, it is possible to estimate the R_S through equation 3.1

$$R_S = \frac{RL}{W} \tag{3.1}$$

The final results are shown in Table 3.2, where it is possible to see that Ti/Au and Cu have similar R_S values for all samples. Al presents higher R_S values than the other metals when deposited over any of the samples studied herein, showing a R_S over MΩ/□ when deposited by thermal evaporation on PDMS (which is a strong indicator of the oxidation of the metal film) and a R_S over 100 Ω/□ when deposited over parylene C.

To evaluate the adhesion of the metals to the substrate, bending and stretching tests were performed. Although the purpose of these films is for wearable devices, and in the vast majority of these applications no large deformations are applied, this study served to evaluate the adhesion of the layers along the test, as well as the corresponding variation

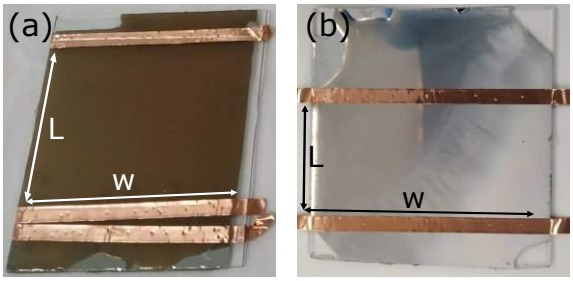

Figure 3.4: Al on PDMS with copper tapes placed on the sample to illustrate how the parameters "L" and "W" are obtained to measure the R_S. (a) Al deposited on PDMS by thermal evaporation; (b) Al deposited on PDMS by E-beam.

Table 3.2: Sheet Resistance of several metals over different substrates after deposition. Abbreviations: NP - Not performed.

Test	Ti/Au	Cu	Al by evaporation	Al by E-beam
R_S (Metal on PDMS, (Ω/□))	1.31	1.36	> 20 (MΩ/□)	3.64
R_S (Metal on Parylene, (Ω/□))	1.07	0.49	116.8	NP
R_S (Metal on Glass, (Ω/□))	0.86	0.58	9.1	NP

of R_S.

3.2.1 Bending Test

This test consisted in bending a film 100 times, 180° (∽1 mm curvature radius) as illustrated in the Figure 3.5. Firstly, the initial R_S was measured, and after bending the film for 10 times, the R_S was measured again and the sample was photographed. This procedure was repeated after the first 25, 50, and 100 bending cycles. The R_S results

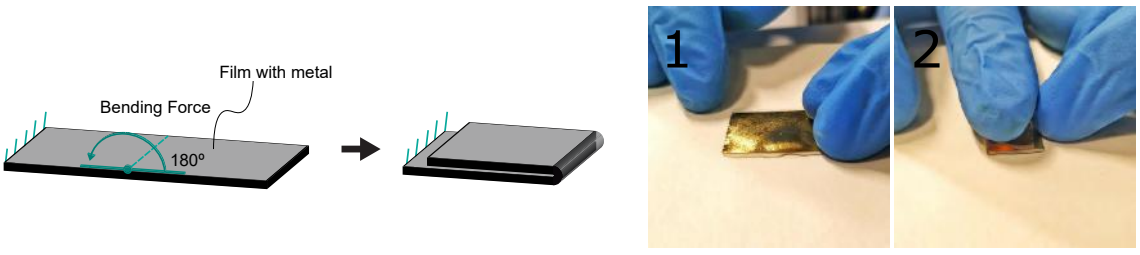

Figure 3.5: Bending test example.

for the PDMS films with different metals are presented in the Table 3.3. Regarding the initial R_S, and comparing with the initial value obtained in Table 3.2, it is possible to see that only Cu samples have a big variation, more than 100 Ω/□. This may be an indicator of the poor adhesion of Cu to PDMS, which is also highlighted in Figure 3.6, where the copper tape would easily detach from PDMS film, removing the copper underneath it. After the first bending cycle, it was also impossible to measure the R_S, despite the copper tape was reattached to the PDMS film. Nevertheless, the bending test was performed

until the 100th cycle, and the photographs of this sample show that the Cu does not show any visible damage after 100 bending cycles.

Unlike Cu, samples with Ti/Au or Al present no visible damage. Ti/Au's R_S did not have a significantly variation throughout this test, but Al R_S increased by.

Table 3.3: Results of the Sheet Resistance of several metals over PDMS throughout the bending test. All metals were deposited by E-beam.

Bending cycle	R_S **of Ti/Au** ($\Omega/\square$)	R_S **of Cu** ($\Omega/\square$)	R_S **of Al** ($\Omega/\square$)
0	1.01	116.07	8.1
10	1.18	No Contact	11.8
25	1.18	No Contact	21.0
50	1.18	No Contact	36.6
100	1.26	No Contact	70.8

Regarding the bending test for metals over Parylene C, the initial R_S was similar to the value shown in Table 3.2 for measurements after the metals deposition, except for Al.

The R_S results are stable for Ti/Au and Cu, while for Al they increased by 130 $\Omega/\square$ throughout the test. All samples presented small horizontal cracks in the bent part of the metal layer. The presence of cracks may be explained by the fact that parylene C is a material with a smaller elasticity than PDMS (with a Young's Modulus of 2.76 MPa and <0.87 MPa, respectively) [24]. All these samples' photographs can be consulted in Appendix A, Figure A.6.

Table 3.4: Results of the Sheet Resistance of several metals over Parylene C throughout the bending test. All metals were deposited by E-beam, except Al by Thermal Evaporation.

Bending Cycle	R_S **of Ti/Au** ($\Omega/\square$)	R_S **of Cu** ($\Omega/\square$)	R_S **of Al** ($\Omega/\square$)
0	1.05	0.36	45
10	1.13	0.36	87
25	1.13	0.36	126
50	1.45	0.48	166
100	2.10	0.83	175

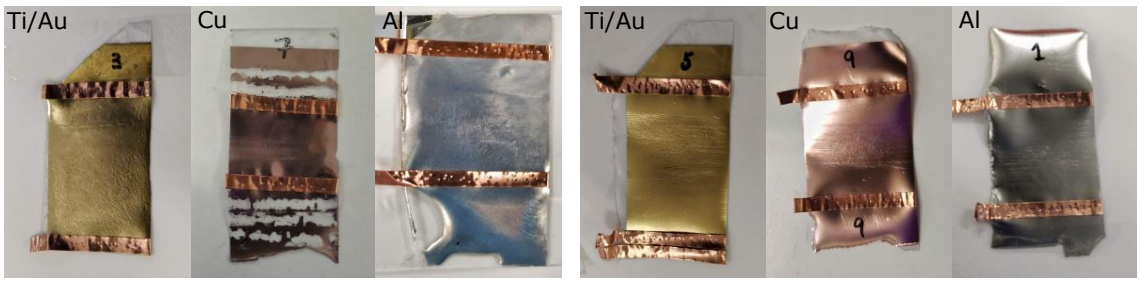

Figure 3.6: On the left, PDMS samples with Ti/Au, Cu, or Al, after 100 bending cycles. On the right, PDMS with parylene C samples with Ti/Au, Cu, or Al, after 100 bending cycles.

3.2.2 Stretching Test

Similar to the bending test, this process consisted of stretching the film with the deposited metal for 100 times, Figure 3.7. The stretching was performed in films with a L=2.5 cm applying a ΔL=0.5 cm stretch, which represents ∽20% a deformation in the sample. The test starts by measuring the R_S before any stretching cycle, and after stretching the film for 10 times, the R_S is measured again and the sample is photographed. This procedure was repeated after the first 25, 50, and 100 bending cycles.

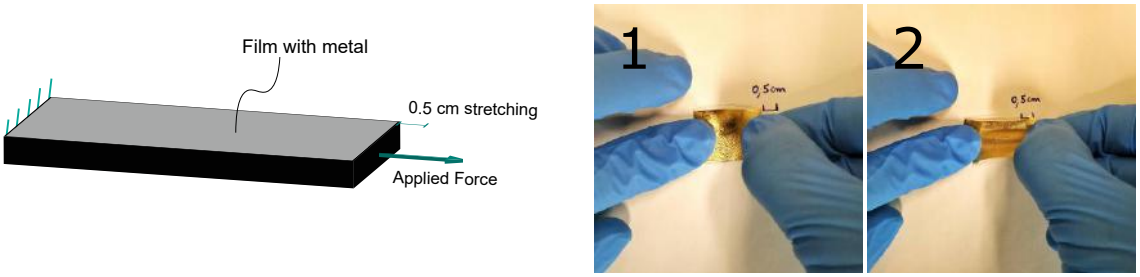

Figure 3.7: Stretching test example.

The R_S results for the PDMS films with different metals are presented in the Table 3.5. Once again, only the Al sample showed a slightly higher (10 Ω/□ higher) initial R_S when compared to the value presented in Table 3.2.

The Ti/Au samples had similar results during the whole test. Similarly to the bending test, the Cu film was removed from PDMS due to the copper tape not being able to withstand the stretching cycles. However, the initial R_S value for Cu layer was quite similar to that shown in Table 3.2. Every PDMS with Al tore up after the 3rd stretching cycle. This is not common in PDMS samples due to its elasticity, so it possibly occurred because this sample was thinner than the other ones. The samples' visual appearance in the end of this process was similar to the beginning, as shown in Figure 3.8 and as expected due to the elasticity properties of PDMS.

Table 3.5: Results of the Sheet Resistance of several metals over PDMS throughout the stretching test. All metals were deposited by E-beam.

Stretching Cycle	R_S **of Ti/Au** (Ω/□)	R_S **of Cu** (Ω/□)	R_S **of Al** (Ω/□)
0	0.84	2.7	14.8
10	1.76	No Contact	Torn
25	2.02	No Contact	Torn
50	1.76	No Contact	Torn
100	2.35	No Contact	Torn

As described before, Parylene C does not have a high elasticity, and for this reason the samples tend to break on the stretching test. Looking to Table 3.6, all samples eventually broke throughout the test. The initial R_S was similar to the other tests with the negligible increase in value in Al sample. The Ti/Au sample was the only one that did not withstand

at least 10 stretching cycles, breaking at the 5th stretch, while Cu broke at the 13th and Al at the 12th stretch. These samples are presented in Figures 3.8.

Table 3.6: Results of the Sheet Resistance of several metals over Parylene C throughout the Stretching Test. All metals were deposited by E-beam.

Stretching Cycle	R_S **of Ti/Au** ($\Omega/\square$)	R_S **of Cu** ($\Omega/\square$)	R_S **of Al** ($\Omega/\square$)
0	1.25	0.36	35
10	Torn	0.71	8000
25	Torn	Torn	Torn
50	Torn	Torn	Torn
100	Torn	Torn	Torn

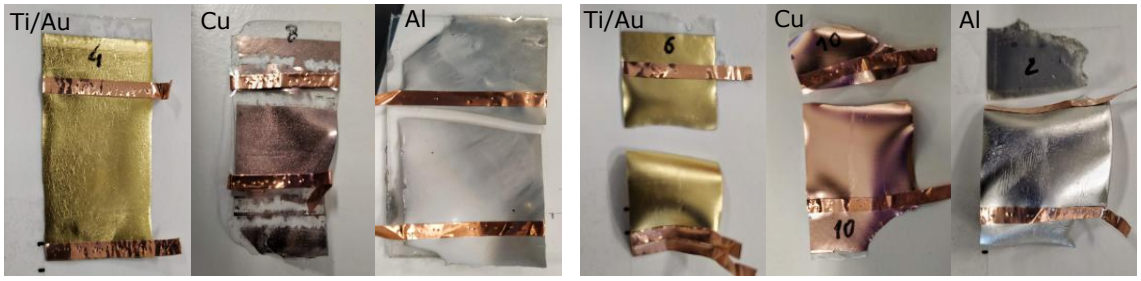

Figure 3.8: On the left, PDMS samples with Ti/Au and Cu after 100 stretching cycles. Al sample broke at the 3rd stretching cycle. On the right, PDMS with parylene C samples with Ti/Au, Cu, or Al, after 5, 13 and 12 stretching cycles respectively.

3.3 Microstructuration film

In order to microstructurate PDMS films, 3 different substrates were tested as molds (acrylic, parylene C, and hard PDMS)

3.3.1 Microstructures by Langmuir Blogett

The technique of deposition of PS spheres by LB turned out to be interesting because this layer of spheres can be used as a mask in a RIE process. The chosen substrate to create the structures was a thin parylene C film deposited on a silicon wafer and acrylic.

Before any deposition was studied the acrylic etching rate by RIE using O_2, with a gas flow of 10 sccm, a power of 50 W, and a pressure of 45 mTorr. Several acrylic samples were subjected to RIE for different periods (from 5 min to 40 min), and the etched thickness was measured using the profilometer. The results are presented in Figure 3.9. The results presented point towards an etching rate of 286 nm/min.

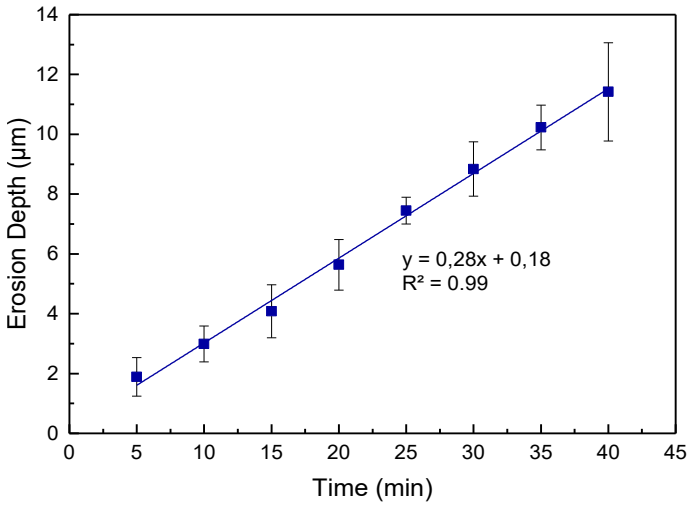

Figure 3.9: (a)Acrylic etching by oxygen plasma using RIE technique.

However, this material showed some problems in the LB process for the reason that was never possible to obtain a homogeneous deposition as shown in Figure 3.10(b).

Using a parylene C film as a substrate opens a range of opportunities, not only to be used as a mold but also as a structured film. The PS spheres used in this work had 4.98 μm ± 0.15 μm, in 10% w/v aqueous suspension. Although it was possible to use smaller diameter spheres, with these spheres it was possible to create bigger domes with a greater spacing, improving the device.

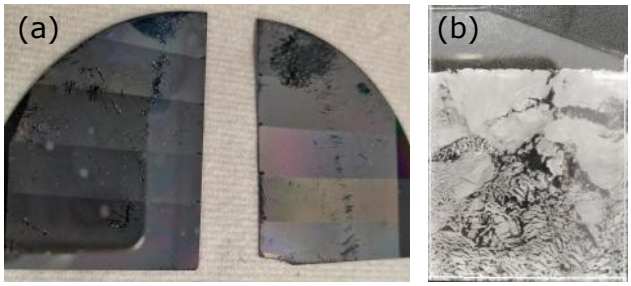

Figure 3.10: (a) Sample of a LB deposition on a silicon wafer with Parylene C after the RIE process for structural study over time; (b) Acrylic sample after deposition by LB process.

To create the structures, an etching process is required, so in order to study the diameter and height of the structures created by the spheres erosion, several LB spheres depositions were made on parylene C, and then subjected to a RIE process with the same parameters applied on the acrylic erosion but with different exposing times (from 3 min to 33 min, in steps of 3 min), as shown in Figure 3.10(a).

The structures created after this process were analyzed to measure their diameter and height using SEM, Figure 3.10(b) . The SEM images of this analysis are presented in Appendix B.

The diameter of the structures (Figure B.4) was measured through *ImageJ Software*, and the results are presented in Figure 3.11. From the analysis of the values, it is possible

to verify that the diameter of the structures decreases around 0.09 μm/min.

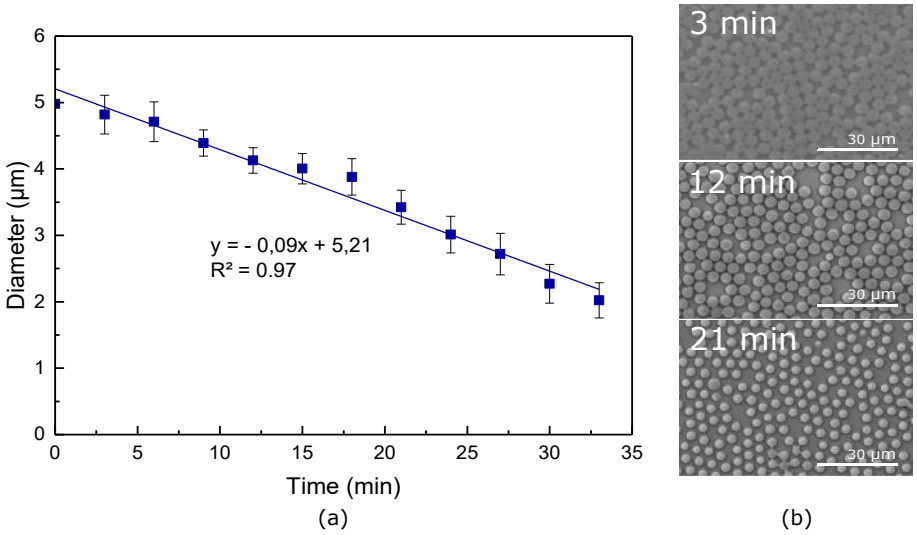

Figure 3.11: (a) Diameter study of the structures created in Parylene C using PS spheres (4.98 μm), deposited by LB, as a mask, for several RIE exposure times; (b) SEM images of diameter variation with etching time.

The height of the dome structures was determined through Figure B.3. The results are presented in Figure 3.12(a), where it can be observed that after an etching of 3 min the structure has a height of 0.22 μm ± 0.04 μm reaching a maximum height of 1.94 μm ± 0.14 μm at 18 min. After 18 min the structures maintain approximately 1.7 μm of height. This is explained by the fact that after 18 min, the PS spheres were already completely etched. Therefore, the parylene C films is etched equally in the top of structures and at their basis, which keeps their height fairly constant. After 33 min of etching the structures were too damaged to get conclusive information about their height.

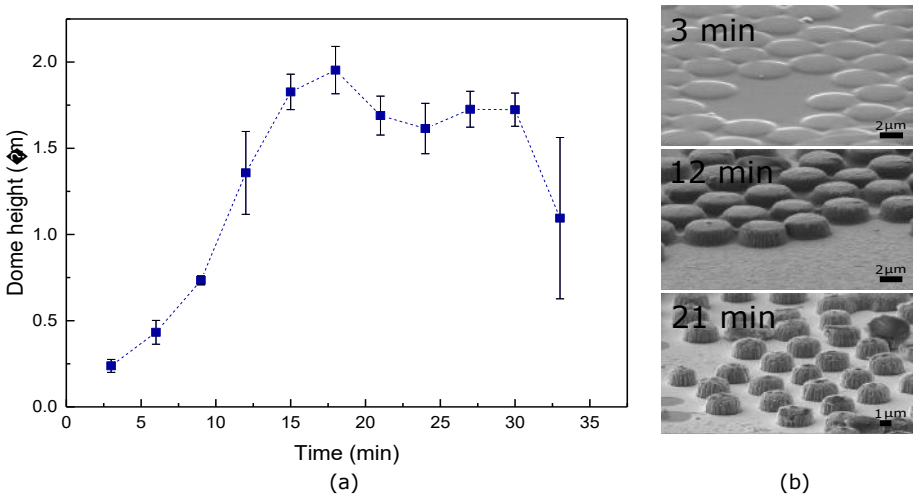

Figure 3.12: (a) Height study of the structures created in parylene C using PS spheres (4.98 μm), deposited by LB, as a mask, for several RIE exposure times; (b) SEM images of height variation with etching time.

In order to produce molds with the negative pattern of the structured parylene C films, a new LB deposition with PS microspheres was made, Figure 3.13a.

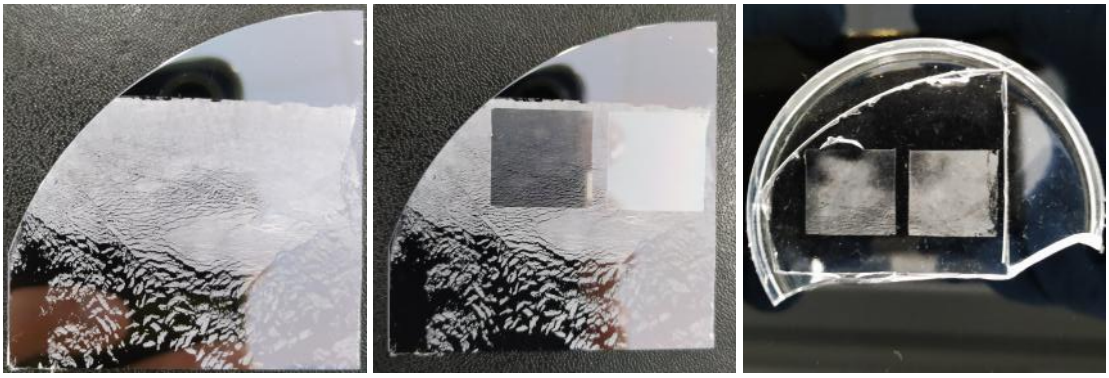

(a) (b) (c)

Figure 3.13: (a) Sample after PS deposition by LB. (b) Sample after RIE etching (left square - 30 min etching; right square - 24 min etching). (c) Hard PDMS mold corresponding to the negative pattern shown in (b).

The parylene C films were etched in a defined area of 2 cm × 2 cm, for 24 min or 30 min, Figure 3.13b, to reach structures with a height of 1.7 μm and a diameter of 2.27 μm or 3 μm, respectively. To obtain a PDMS film with these microstructures it was necessary to produce a negative mold of the parylene C structures. Therefore, the structured parylene C films were covered with PDMS with an elastomer to curing agent ratio of 5:1, which was then cured and detached from parylene (Figure 3.13c).

3.3.2 Microstructures in Si by photolitography

To create a pyramidal mold, a photolitography process followed by wet etching was used. Masks were created with an array of squares of 50 μm and 100 μm, which were used to pattern photoresist by photolithography, followed by an anisotropic erosion with KOH, thus creating cavities with the shape of inverted pyramids. The substrates used for the creation of these structures were silicon wafers coated with 100nm silicon oxide (SiO_2) or 150 nm thickness silicon nitride (Si_3N_4). Theoretically, it is possible to obtain the height of the pyramidal structures through equation 3.2, since anisotropic erosion in silicon is done at an angle of 54.7°. Therefore, knowing the square width (a) and multiplying by 0.707, the depth of the pyramidal cavity (h) is obtained:

$$h = a \times 0.707 \tag{3.2}$$

Table 3.7 presents the theoretical results about the pyramidal cavities' depth through this equation, as well as the real depths achieved.

The photolithography process was made in several samples using masks with different square sizes (100 μm and 50 μm). The anisotropic wet etching was made with KOH at 85 °C, and the respective etching times are shown in Table 3.7. The etching on the samples

Table 3.7: Theoretical and Real equation, as well as the real depths achieved of pyramidal cavities.

Sample	**Squares** (μm)	**Expected height** (μm)	**Real height** (μm)	**Etching Time (min)**
Si_3N_4	50	35.35	37.08 ± 2.67	83
SiO_2	50	35.35	33.57 ± 2.76	92
Si_3N_4	100	70.7	66.43 ± 3.40	122
SiO_2	100	70.7	35.64 ± 2.03	150

with 100 μm squares was interrupted before reaching without reach the expected depth value and forming the pyramid because the squares of the mask were too close and upon etching, the cavities started to merge together.

When the etching process was completed to create the molds, these were silanized and the PDMS deposition was made on them followed by the peel-off process, Figure 3.14. The structures were analyzed by SEM and through the cross-section images, Figure C.1, their height was determined (Table 3.7).

Figure 3.14: Left, mold of Si_3N_4 patterned with squares of 50 μm with SEM view; Right, SEM image (tilted and top view) of pyramids patterned on PDMS, from the respective mold, after peel-off.

3.4 Device development

3.4.1 Piezoresistive sensors

The sensor was assembled by sandwiching two microstructured films either with dome-shape or pyramids, with a Ti/Au electrode, 3.15(a),(b). After assembly, the sensor is connected in series to an auxiliar resistor where, using an oscilloscope, the variation in current, when pressure is applied to the sensor, can be measured 3.15(c). To apply pressure in the sensors, a 1×1 cm base frame was used where weights can be added. The base frame itself applies a 277 Pa pressure to the sensor and weights have been placed up to a maximum pressure of 30.3 kPa, Figure 3.15(d). The measurements were repeated 4 times to ensure reliable sensor response with pressure changes. The sensors were tested for their sensitivity as defined in Equation 3.3 where S is the sensitivity, ΔR corresponds to the resistance change, R_0 is the initial resistance of each sensor in the absence of a pressure, and P is the compressive pressure.

$$S = \frac{d(\frac{\Delta R}{R_0})}{dP} \tag{3.3}$$

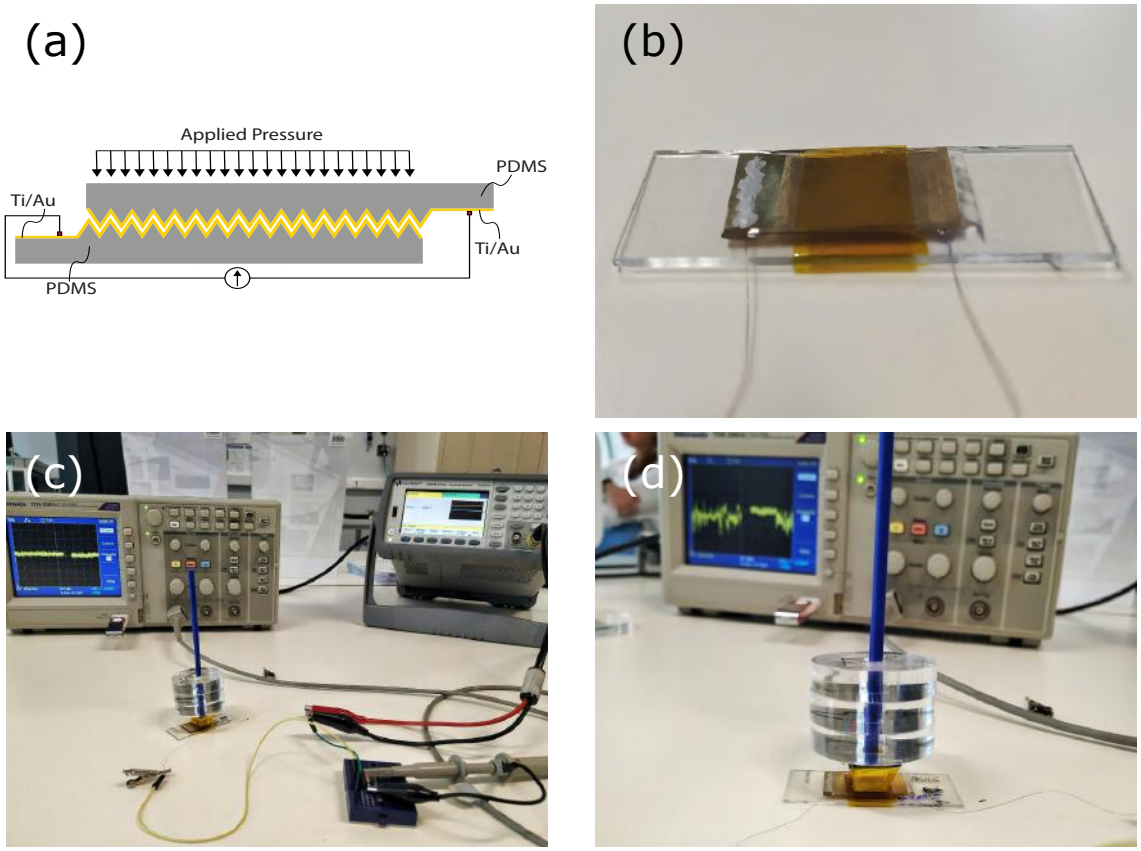

Figure 3.15: (a) schematic of a piezoresistive sensor; (b) Example of a produced piezoresistive sensor; (c) Mounting for measuring sensor resistance variation; (d) Example of the weight support for applying pressure to the device.

Figure 3.16 shows the relative resistance change of the dome-shaped sensors. To better explain the results, from now on the dome-shaped sensor 2.27 μm domes diameter will be referred as "SD sensor", and the 3 μm dome diameter sensor will be "LD sensor", both sensors have the same height (1.70 μm).

Before starting the test R_0 was measured on each sensor with a multimeter, showing the values of 7.50 Ω for SD and 8.3 Ω for LD sensor. When a low-pressure from 0 to 1.30 kPa is applied on these sensors the sensitivity is -5.8×10^{-3} kPa^{-1} for SD sensor, and -1.9×10^{-2} kPa^{-1} for LD sensor. If a high-pressure is applied on the sensor, from 3.28 kPa to 30.3 kPa, the sensitivity decreases, -5.1×10^{-5} kPa^{-1} for SD sensor, and -1.3×10^{-4} kPa^{-1} for LD sensor.

LD sensor presents better sensivity results comparing with SD sensor, by the fact of their structures are less compressible due to their larger diameter, being able to withstand higher pressures [4]. However, the sensitivities obtained for high pressures in LD do not present a linear tendency, which does not lead us to obtain a clear view on the sensitivity

of this device to these pressures. During the work of this dissertation there was no time to study the low pressure regimes in more detail.

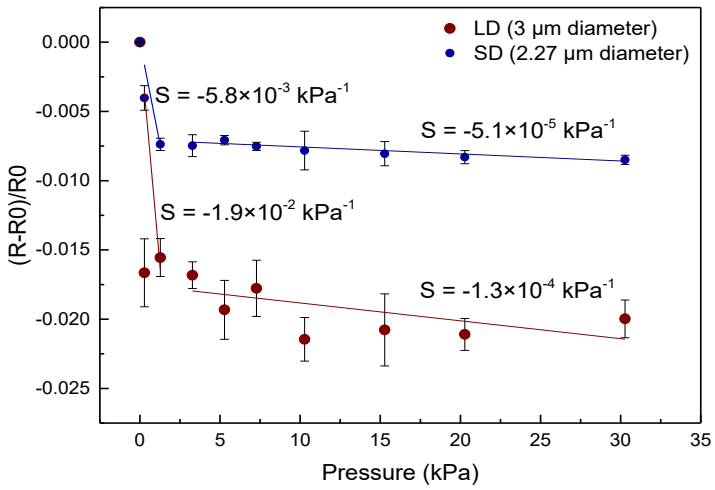

Figure 3.16: Experimental results of the relative resistance change of dome-shaped piezoresistive devices with with 1.70 μm height and different diameters, under a pressure from 277 Pa to 30.3 kPa.

Figure 3.17 shows the relative resistance change of the pyramidal shape sensors for a pressure range from 277 Pa to 30.3 kPa.

Similar to the previous sensors, hereafter, the 35.64 μm height pyramidal sensor will be called "SP sensor" and the sensor with 66.4 μm heigh "LP sensor".

The R_0 for each sensor showed the values of 7 Ω for SP sensor and 8.3 Ω for LP sensor. When the same low-pressure rage (0 to 1.28 kPa) is applied on these sensors the sensitivity is -3.6×10^{-3} kPa^{-1} for SP sensor, and -1.1×10^{-2} kPa^{-1} for LP sensor. In the high-pressure range (3.28 kPa to 30.3 kPa), the sensitivity decreases, -2.2×10^{-5} kPa^{-1} for SP sensor, and -7.7×10^{-5} kPa^{-1} for LP sensor.

These results show that both sensitivity and pressure range are tunable by modifying the shape of the PDMS structures [15].

In the literature it has been reported that pyramidal microstructures are very sensitive to low pressures, but this sensitivity decreases with the application of higher pressures, this can be explained by the micro-structures complete deformation [2, 26]. Also in literature, sensitivity results for this kind of microscructured devices present better results, comparing with the devices developed in this work (-5.4×10^{-1} kPa^{-1} [4]; -15.1 kPa^{-1} [19]; 56.8 kPa^{-1} [2]). The low sensitivity of the sensors tested in this thesis compared with the literature, can be explained by the fact that the initial resistance is too low, this leaves a small resistance variation range when pressure is applied to the sensor. As future work the initial resistance should be increased.

Dome-shaped structures thus show a slight improvement in sensitivity results when

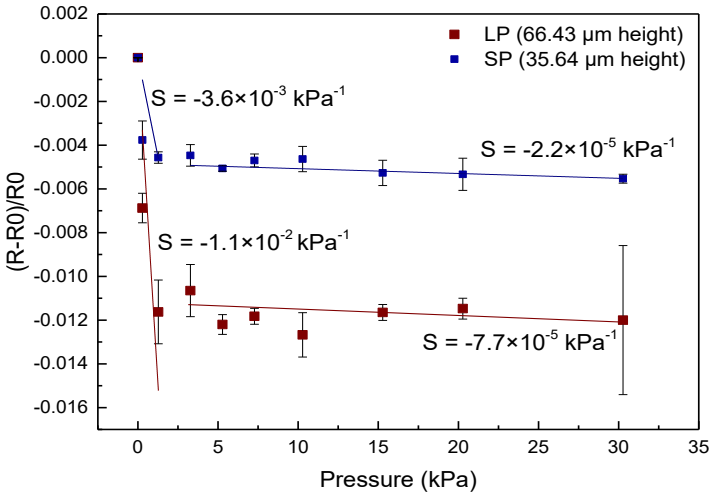

Figure 3.17: Experimental results of the relative resistance change of piezoresistive devices with 35.64 μm, and 66.43 μm height pyramids, under a pressure from 277 Pa to 30.3 kPa.

comparing with pyramids-shaped structures, however, the fact that the size of the structures is so different does not make the devices comparable.

3.4.2 Capacitive sensors

The capacitive pressure sensor consists in two layers of different materials. Unlike the previous sensor, this uses a single microstructured PDMS film. In the first layer, a Ti/Au film was deposited on the opposite side of the microstructures, which will act as the electrode. The second layer has an ITO coated PET substrate, where the ITO is in contact with the microstructures of the previous layer, Figure 3.18. The sensor studied in this work was patterned with 100 μm squares pyramids and a height of 35.64 μm

The circuit to test the capacitive sensor was composed by a Lock-In Amplifier assembled with the sensor and an oscilloscope. The Lock-In measures the current module, applying a voltage of 100 mV and 5 kHz frequency while the oscilloscope detects voltage variation in the sensor with applied pressure. Capacitance can be calculated by the Equation 3.4 where C is the capacitance, I is the current module measured in the Lock-In, V is the voltage module applied by the Lock-In and ω is the angular frequency.

$$C = \frac{I}{V \times \omega} \tag{3.4}$$

The initial capacitance (C_0) was measured with no pressure applied on the sensor, obtaining the value of 21.1 pF, close to the theoretical value calculated by the Equation 1.1 presented in the Section 1.2 (15.1pF). The used parameters to calculate the theoretical value were, PDMS dielectric permittivity 2.34 [27], distance between the electrodes (PDMS thickness plus microstructures) ~137 μm and the electrode area 1 cm^2.

The process to apply pressure in the sensor was similar to the piezoresistive test, Figure 3.15(d), varying pressures between 0 to 4.28 kPa, and the measurements were

repeated 4 times to ensure reliable sensor response with pressure changes. The sensors were tested for their sensitivity as defined in Equation 3.5 where S is the sensitivity, ΔC corresponds to the resistance change, C_0 is the initial resistance of each sensor in the absence of a pressure, and P is the compressive pressure.

$$S = \frac{d(\frac{\Delta C}{C_0})}{dP} \tag{3.5}$$

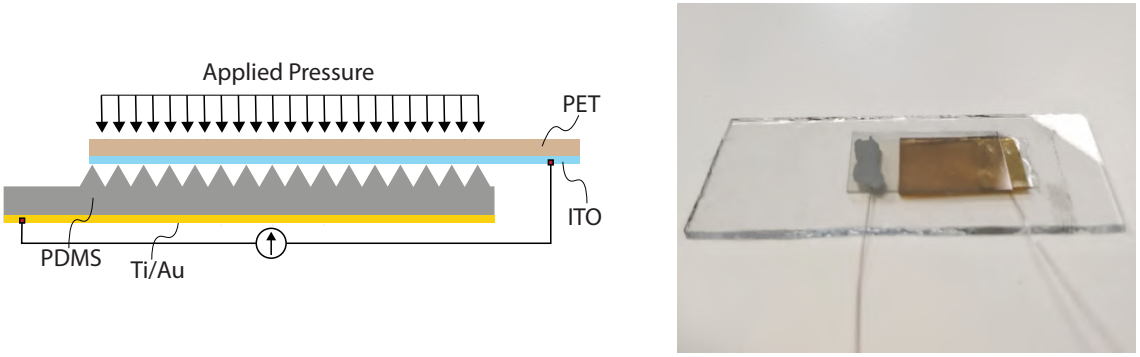

Figure 3.18: In the left the schematic of a capacitive sensor, and in the right, the capacitive sensor produced.

The sensivity results for low pressures (0 to 0.98 kPa) were 3.1×10^{-2} kPa^{-1} and for high pressures (1.28 kPa to 4,28 kPa) 7.1×10^{-3} kPa^{-1}, Figure 3.19.

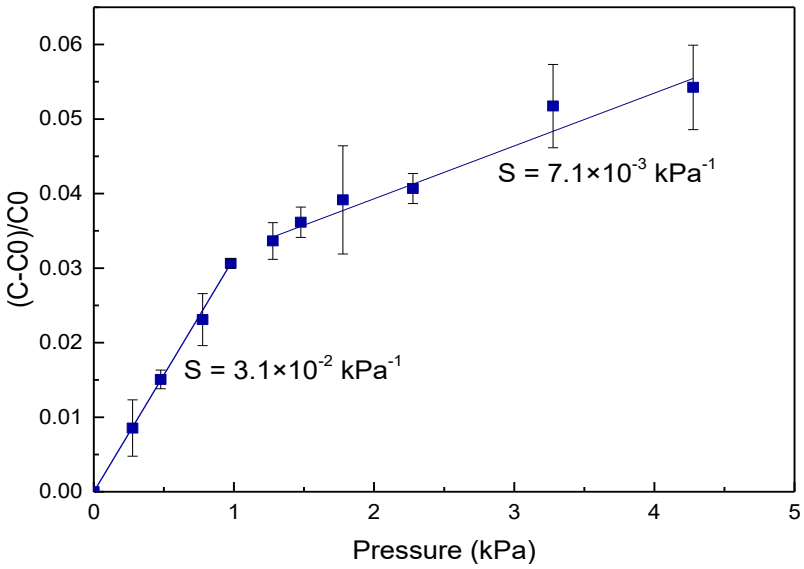

Figure 3.19: Relative resistance change of a piezoresistive device with 35.64 μm height pyramids, under a pressure from 0 to 4.28 kPa.

In the low pressure range, the sensitivity is determined mostly by the sensor's microstructural features since changes in the bulk material thickness would be negligible at

lower pressure changes [25]. For pressures higher than 1.28 kPa the sensitivity decreases, this fact can be explained to the increasing elastic resistance with increasing compression. In higher loads is not required a high senitivity, and this progressive damping increases the range of detectable pressure what is usefull for some real-world applications [15].

The sensitivity results obtained are comparable with values reported in the literature for sensors with pyramidal microstrutures (2.2×10^{-2} kPa^{-1} [25]).

Comparing the piezoresistive and capacitive devices studied in this work, the capacitive sensor presented better sensitivity results to pressures under 4,28 kPa, however, this sensor tends to saturate after 5 kPa pressures, while the piezoresistive sensor is capable of obtaining some sensitivity, although very poor, up to 30.3 kPa pressures. This can be explained by the fact that the capacitive sensor has a bigger range to vary ΔC by the deformation of the structures when pressure is applied than the range of the piezoresistive sensors of this work to vary ΔR.

Chapter 4

Conclusions and Future Perspectives

The present work was focused on study the process to create molds to pattern microstruturated films as well as study the films properties in order to produce pressure sensors.

In the beginning of the work, a PDMS film study was carried out, where was concluded that its possible to control PDMS film thickness by varying the spinner rotation value during the spin-coating process. After this study, several PDMS films samples with different thicknesses were created in order to test the ease with which film is peeled-off from the substrate, where it was concluded that is very difficult to peel-off films under 21 μm thickness. As an alternative to substrate silanization to facilitate peel-off, the possibility of using a PVA layer before PDMS film deposition was studied, which had no evident advantages compared to the silanization process. For the parylene C films thickness also studied, it was concluded that its thickness can be controlled with high precision in a linear way with the dimer mass.

Since PDMS presents some difficulties in metal adhesion due to its low surface energy, metal (Al, Cu and Ti/Au) deposition tests were performed successfully in high vacuum by E-beam without any PDMS treatment before. During these metal depositions, was simultaneously deposited on a parylene C thin film (previously deposited on PDMS), which proved to be an excellent substrate for metal adhesion. Both, PDMS and PDMS with Parylene C films were tested in mechanical bending and stretching tests (10, 25, 50 and 100 cycles) and electrically characterized for their sheet resistance in the beginning and in the end of each cycle. Ti/Au in both tests and substrates did not show large sheet resistance variations (~2 Ω/□). In a different way, Al presented large sheet resistance variations after cycles (>60 Ω/□). Cu deposited on PDMS presented a problem when copper tape was glued to the surface, pelling off the metal, the same was not observed for Cu deposited on parylene C. In particular, the parylene C as substrate could not stand the stretching tests, torning in all samples, this is explained by the high young modulus and low elongation to break percentage, compared with PDMS.

From the 2 substrates studied to produce a microstructure mold using the LB technique, acrylic was not a good option, presenting difficulties in the PL microspheres adhesion to its surface, but with parylene C it was possible make depositions and, after

studying the dome-shaped microstrutures formed by the RIE process, establish a relationship between exposure time and structure size. Was possible to conclude that the structures decreases around 0.09 μm/min and a maximum height of 1.94 μm. Nevertheless, the LB technique is difficult to control, and it is not possible to obtain equal samples in different depositions. As for the pyramid-shaped structures, in a future mechanical masks designing process the squares should be redrawn with a distance between them greater than the square-side value. The squares drawn in this work were too close between them, and for this reason, the anisotropic wet etching had some problems for the 100 μm squares-side.

Piezoresistive pressure sensors with sensitivity of -1.9×10^{-2} kPa^{-1} were achieved for a pressure range lower than 1.28 kPa, and with -1.3 ×10^{-4} kPa^{-1} for a pressure range from 3.28 kPa to 30.28 kPa. The low sensitivity achieved on these sensors is due to a very low initial resistance (8.3 Ω) which does not allow a higher ΔR when pressure is applied to the sensor. In future works the electrode resistance has to be higher, using a different material or introducing some material into the PDMS mixture that makes it conductive. Capacitive pressure sensors with a sensitivity of 3.1×10^{-2} kPa^{-1} for pressures below 0.98 kPa, and 7.1 ×10^{-3} kPa^{-1} for pressures between 1.23 kPa and 4.28 kPa, were also achieved. This sensor has been shown to be in a range of sensitivity comparable to some similar recently studied sensors [25].

As a future perspective, parylene C has proved to be a very interesting material to introduced in wearables, is as it is compatible with lithographic processes and showed good results in the studies in this thesis.

Bibliography

[1] B. Balakrisnan, S. Patil, and E. Smela. "Patterning PDMS using a combination of wet and dry etching." In: *Journal of Micromechanics and Microengineering* 19.4 (2009), p. 047002.

[2] C.-L. Choong, M.-B. Shim, B.-S. Lee, S. Jeon, D.-S. Ko, T.-H. Kang, J. Bae, S. H. Lee, K.-E. Byun, J. Im, et al. "Highly stretchable resistive pressure sensors using a conductive elastomeric composite on a micropyramid array." In: *Advanced materials* 26.21 (2014), pp. 3451–3458.

[3] C. Dagdeviren, Y. Su, P. Joe, R. Yona, Y. Liu, Y.-S. Kim, Y. Huang, A. R. Damadoran, J. Xia, L. W. Martin, et al. "Conformable amplified lead zirconate titanate sensors with enhanced piezoelectric response for cutaneous pressure monitoring." In: *Nature communications* 5 (2014), p. 4496.

[4] A. Dos Santos, N. Pinela, P. Alves, R. Santos, R. Farinha, E. Fortunato, R. Martins, H. Águas, and R. Igreja. "E-skin bimodal sensors for robotics and prosthesis using PDMS molds engraved by laser." In: *Sensors* 19.4 (2019), p. 899.

[5] F.-R. Fan, L. Lin, G. Zhu, W. Wu, R. Zhang, and Z. L. Wang. "Transparent triboelectric nanogenerators and self-powered pressure sensors based on micropatterned plastic films." In: *Nano letters* 12.6 (2012), pp. 3109–3114.

[6] S. Gong, W. Schwalb, Y. Wang, Y. Chen, Y. Tang, J. Si, B. Shirinzadeh, and W. Cheng. "A wearable and highly sensitive pressure sensor with ultrathin gold nanowires." In: *Nature communications* 5 (2014), p. 3132.

[7] M. L. Hammock, A. Chortos, B. C.-K. Tee, J. B.-H. Tok, and Z. Bao. "25th anniversary article: the evolution of electronic skin (e-skin): a brief history, design considerations, and recent progress." In: *Advanced materials* 25.42 (2013), pp. 5997–6038.

[8] C. Hassler, T. Boretius, and T. Stieglitz. "Polymers for neural implants." In: *Journal of Polymer Science Part B: Polymer Physics* 49.1 (2011), pp. 18–33.

[9] Y. R. Jeong, H. Park, S. W. Jin, S. Y. Hong, S.-S. Lee, and J. S. Ha. "Highly stretchable and sensitive strain sensors using fragmentized graphene foam." In: *Advanced Functional Materials* 25.27 (2015), pp. 4228–4236.

[10] Y. Joo, J. Byun, N. Seong, J. Ha, H. Kim, S. Kim, T. Kim, H. Im, D. Kim, and Y. Hong. "Silver nanowire-embedded PDMS with a multiscale structure for a highly sensitive and robust flexible pressure sensor." In: *Nanoscale* 7.14 (2015), pp. 6208–6215.

[11] S. Kuppusami and R. H. Oskouei. "Parylene coatings in medical devices and implants: A review." In: *Universal Journal of Biomedical Engineering* 3.2 (2015), pp. 9–14.

[12] K. S. Lim, W.-J. Chang, Y.-M. Koo, and R. Bashir. "Reliable fabrication method of transferable micron scale metal pattern for poly (dimethylsiloxane) metallization." In: *Lab on a Chip* 6.4 (2006), pp. 578–580.

[13] Z. Lou, S. Chen, L. Wang, R. Shi, L. Li, K. Jiang, D. Chen, and G. Shen. "Ultrasensitive and ultraflexible e-skins with dual functionalities for wearable electronics." In: *Nano Energy* 38 (2017), pp. 28–35.

[14] A. R. Madaria, A. Kumar, F. N. Ishikawa, and C. Zhou. "Uniform, highly conductive, and patterned transparent films of a percolating silver nanowire network on rigid and flexible substrates using a dry transfer technique." In: *Nano Research* 3.8 (2010), pp. 564–573.

[15] S. C. Mannsfeld, B. C. Tee, R. M. Stoltenberg, C. V. H. Chen, S. Barman, B. V. Muir, A. N. Sokolov, C. Reese, and Z. Bao. "Highly sensitive flexible pressure sensors with microstructured rubber dielectric layers." In: *Nature materials* 9.10 (2010), p. 859.

[16] I. d. O. Martins. "Parylene C as substrate, dielectric and encapsulation for flexible electronics applications." Master's thesis. Faculdade de Ciências e Tecnologia da Universidade Nova de Lisboa, 2017.

[17] A. Mata, A. J. Fleischman, and S. Roy. "Characterization of polydimethylsiloxane (PDMS) properties for biomedical micro/nanosystems." In: *Biomedical microdevices* 7.4 (2005), pp. 281–293.

[18] C. Pang, T.-i. Kim, W. G. Bae, D. Kang, S. M. Kim, and K.-Y. Suh. "Bioinspired Reversible Interlocker Using Regularly Arrayed High Aspect-Ratio Polymer Fibers." In: *Advanced Materials* 24.4 (2012), pp. 475–479.

[19] J. Park, Y. Lee, J. Hong, M. Ha, Y.-D. Jung, H. Lim, S. Y. Kim, and H. Ko. "Giant tunneling piezoresistance of composite elastomers with interlocked microdome arrays for ultrasensitive and multimodal electronic skins." In: *ACS nano* 8.5 (2014), pp. 4689–4697.

[20] J. Park, Y. Lee, J. Hong, Y. Lee, M. Ha, Y. Jung, H. Lim, S. Y. Kim, and H. Ko. "Tactile-direction-sensitive and stretchable electronic skins based on human-skin-inspired interlocked microstructures." In: *ACS nano* 8.12 (2014), pp. 12020–12029.

[21] J. Park, M. Kim, Y. Lee, H. S. Lee, and H. Ko. "Fingertip skin–inspired microstructured ferroelectric skins discriminate static/dynamic pressure and temperature stimuli." In: *Science advances* 1.9 (2015), e1500661.

[22] J. Park, Y. Lee, M. Ha, S. Cho, and H. Ko. "Micro/nanostructured surfaces for self-powered and multifunctional electronic skins." In: *Journal of Materials Chemistry B* 4.18 (2016), pp. 2999–3018.

[23] M. Park, H. Kim, and J. P. Youngblood. "Strain-dependent electrical resistance of multi-walled carbon nanotube/polymer composite films." In: *Nanotechnology* 19.5 (2008), p. 055705.

[24] D. C. Rodger. "Development of flexible Parylene-based microtechnologies for retinal and spinal cord stimulation and recording." Doctoral dissertation. California Institute of Technology, 2008.

[25] S. R. A. Ruth, L. Beker, H. Tran, V. R. Feig, N. Matsuhisa, and Z. Bao. "Rational Design of Capacitive Pressure Sensors Based on Pyramidal Microstructures for Specialized Monitoring of Biosignals." In: *Advanced Functional Materials* (2019), p. 1903100.

[26] A. dos Santos, N. Pinela, P. Alves, R. Santos, E. Fortunato, R. Martins, H. Águas, and R. Igreja. "Piezoresistive E-Skin Sensors Produced with Laser Engraved Molds." In: *Advanced Electronic Materials* 4.9 (2018), p. 1800182.

[27] G. Schwartz, B. C.-K. Tee, J. Mei, A. L. Appleton, D. H. Kim, H. Wang, and Z. Bao. "Flexible polymer transistors with high pressure sensitivity for application in electronic skin and health monitoring." In: *Nature communications* 4 (2013), p. 1859.

[28] M.-L. Seol, J.-H. Woo, D.-I. Lee, H. Im, J. Hur, and Y.-K. Choi. "Nature-Replicated Nano-in-Micro Structures for Triboelectric Energy Harvesting." In: *Small* 10.19 (2014), pp. 3887–3894.

[29] D. Son, J. Lee, S. Qiao, R. Ghaffari, J. Kim, J. E. Lee, C. Song, S. J. Kim, D. J. Lee, S. W. Jun, et al. "Multifunctional wearable devices for diagnosis and therapy of movement disorders." In: *Nature nanotechnology* 9.5 (2014), p. 397.

[30] G. Torrisi, J. S. Luis, O. Sanchez-Sobrado, R. Raciti, M. J. Mendes, H. Águas, E. Fortunato, R. Martins, and A. Terrasi. "Colloidal-structured metallic micro-grids: High performance transparent electrodes in the red and infrared range." In: *Solar Energy Materials and Solar Cells* 197 (2019), pp. 7–12.

[31] X. Wang, Y. Gu, Z. Xiong, Z. Cui, and T. Zhang. "Silk-molded flexible, ultrasensitive, and highly stable electronic skin for monitoring human physiological signals." In: *Advanced materials* 26.9 (2014), pp. 1336–1342.

[32] C. Yu, C. Masarapu, J. Rong, B. Wei, and H. Jiang. "Stretchable supercapacitors based on buckled single-walled carbon-nanotube macrofilms." In: *Advanced Materials* 21.47 (2009), pp. 4793–4797.

[33] X. Zeng, Z. Wang, H. Zhang, W. Yang, L. Xiang, Z. Zhao, L.-M. Peng, and Y. Hu. "Tunable, ultrasensitive, and flexible pressure sensors based on wrinkled microstructures for electronic skin." In: *ACS applied materials & interfaces* (2019).

[34] Z. Zhang, L. Li, J. Horng, N. Z. Wang, F. Yang, Y. Yu, Y. Zhang, G. Chen, K. Watanabe, T. Taniguchi, et al. "Strain-modulated bandgap and piezo-resistive effect in black phosphorus field-effect transistors." In: *Nano letters* 17.10 (2017), pp. 6097–6103.

Appendix A

On this appendix are presented photographs of all the metal depositions by E-beam on PDMS, and Parylene coated PDMS membranes, as well as photos of the mechanical bending and stretching tests after the respective cycles.

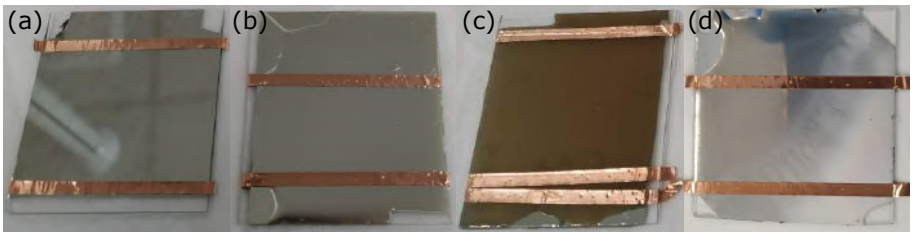

Figure A.1: Samples with deposited Al and copper tape. (a) Al deposited on Glass; (b) Al deposited on PDMS with Parylene C; (c) Al deposited on PDMS; (d) Al deposited on PDMS. Al was deposited by thermal evaporation on samples (a) to (c) and by E-beam on sample (d).

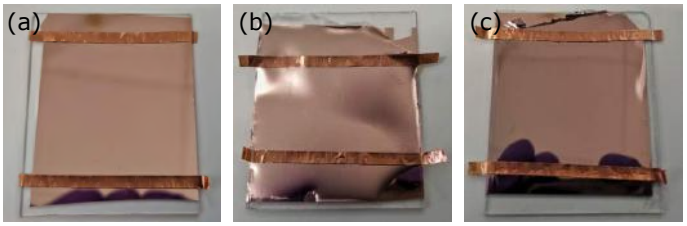

Figure A.2: Samples with deposited Cu and copper tape. (a) Cu deposited on Glass; (b) Cu deposited on PDMS with Parylene C; (c) Cu deposited on PDMS. Cu was deposited by E-beam on all samples.

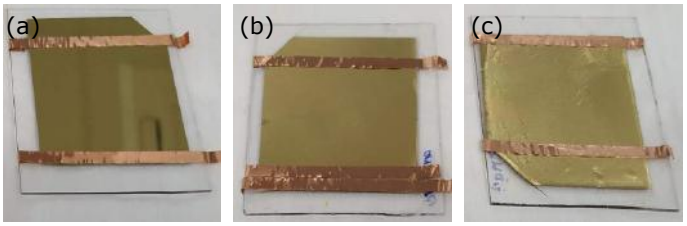

Figure A.3: Samples with deposited Ti/Au and copper tape. (a) Ti/Au deposited on Glass; (b) Ti/Au deposited on PDMS with Parylene C; (c) Ti/Au deposited on PDMS. Ti/Au was deposited by E-beam on all samples.

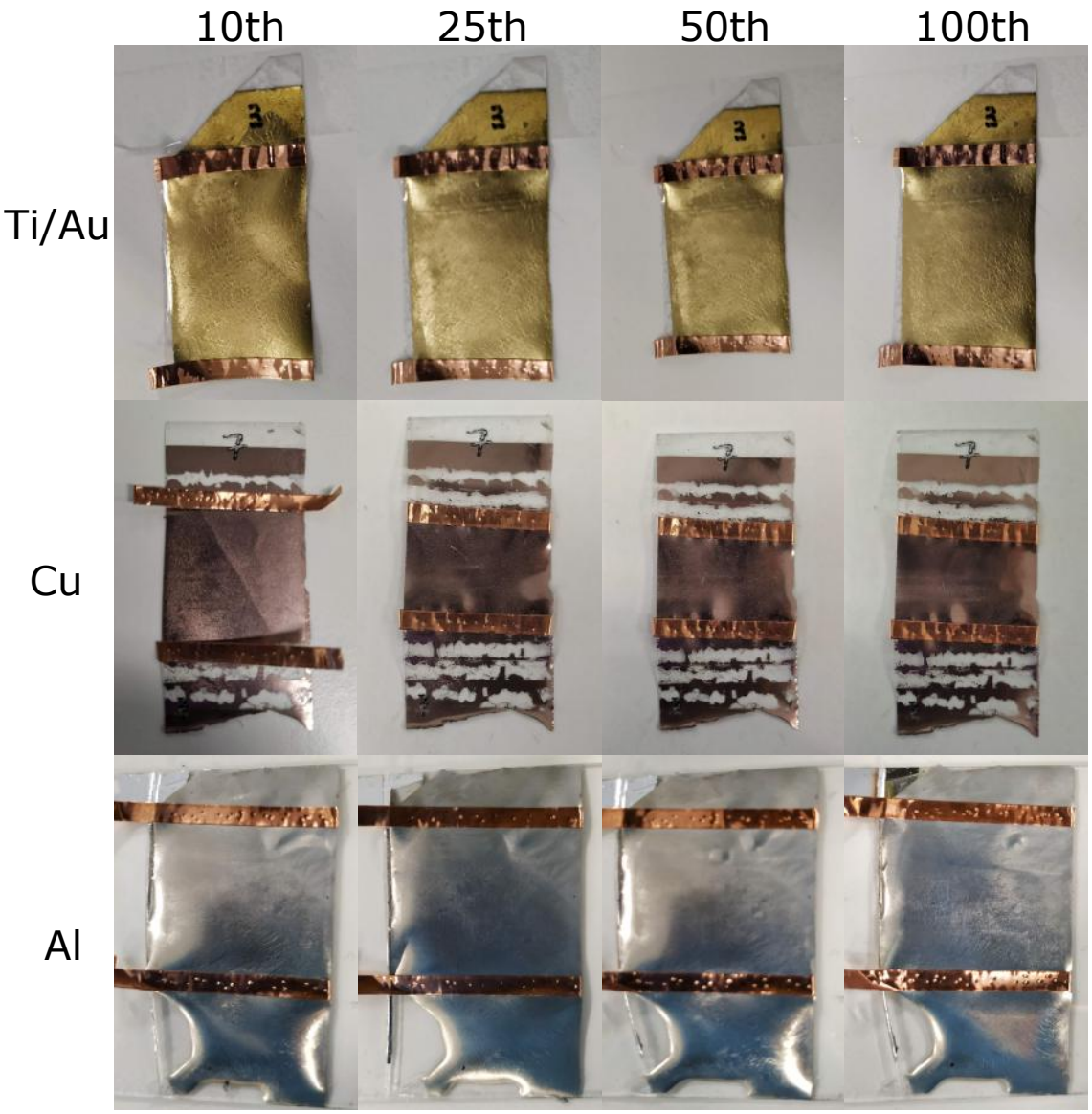

Figure A.4: PDMS samples with Ti/Au, Cu, or Al, after bending cycles (10, 25, 50, and 100).

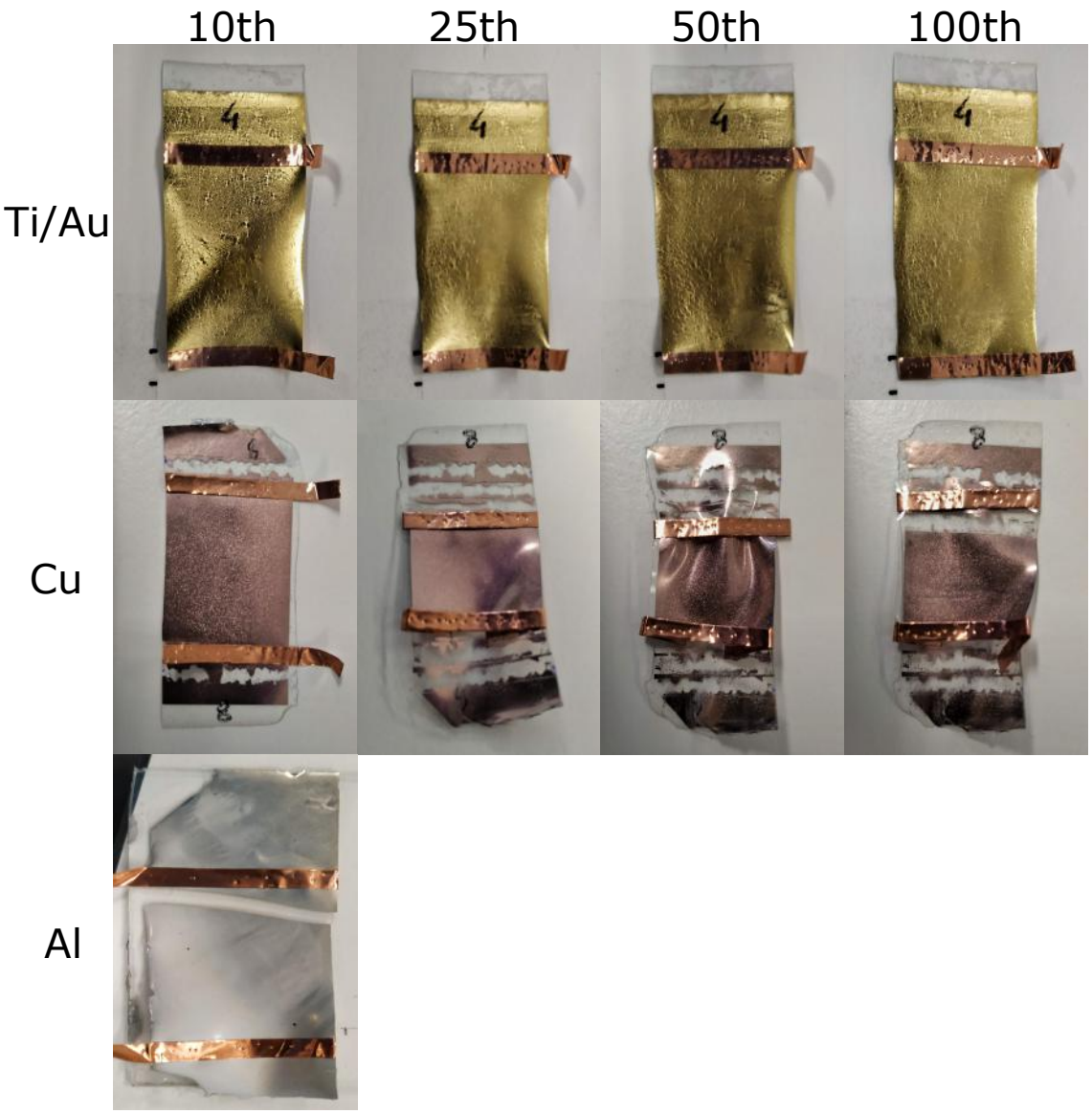

Figure A.5: PDMS samples with Ti/Au, Cu, or Al, after stretching cycles (10, 25, 50, and 100). The Al sample broke at the 3rd stretching cycle.

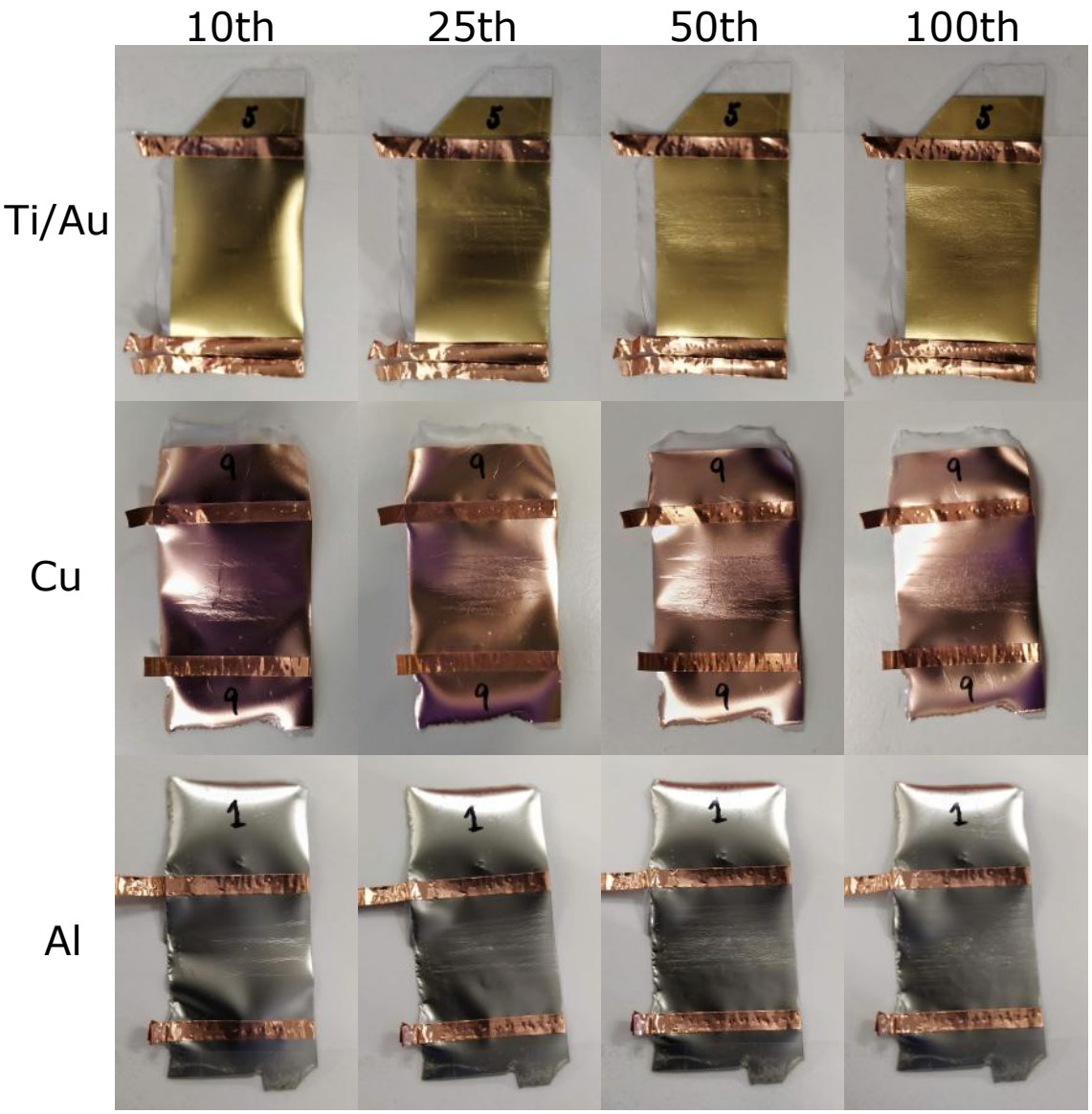

Figure A.6: PDMS with parylene C samples with Ti/Au, Cu, or Al, after bending cycles (10, 25, 50, and 100).

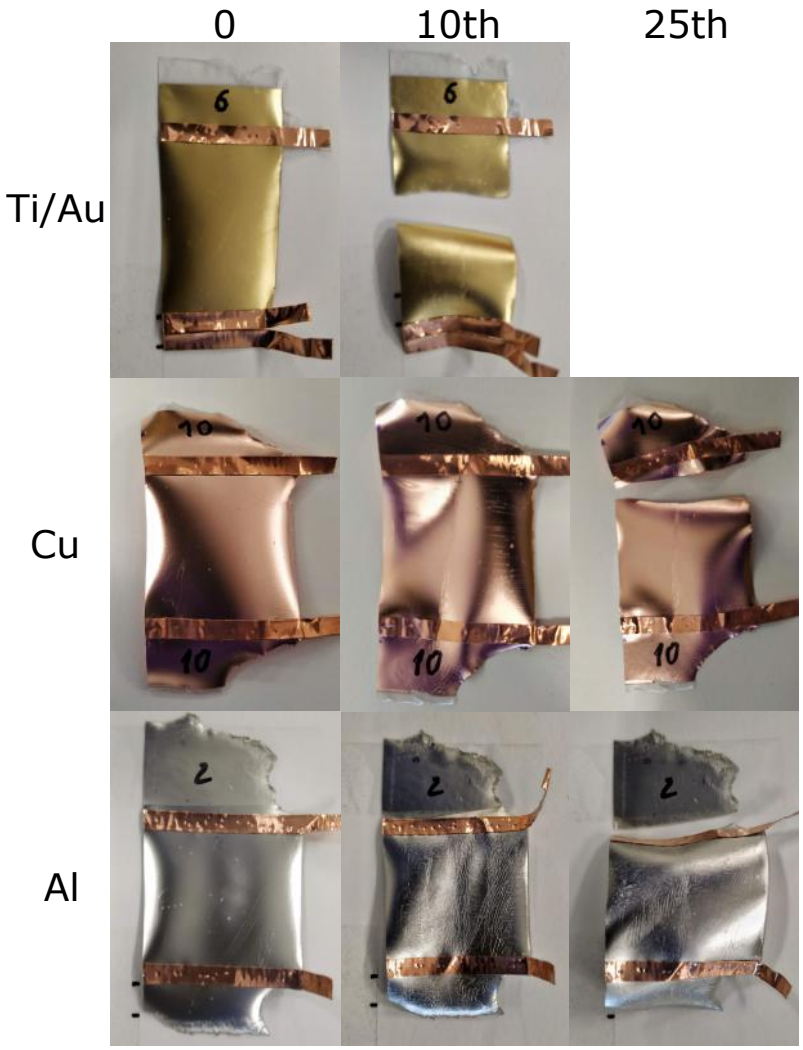

Figure A.7: PDMS with parylene C samples with Ti/Au, Cu, or Al, after stretching cycles (0, 10, and 25). The Ti/Au sample broke at the 5th stretching cycle, Cu at the 13th and Al at the 12th.

APPENDIX B

In this appendix are presented the processes schematics of the used technics to reach the dome-shape structures, as well as the SEM images of the domes created in Parylene C by these processes.

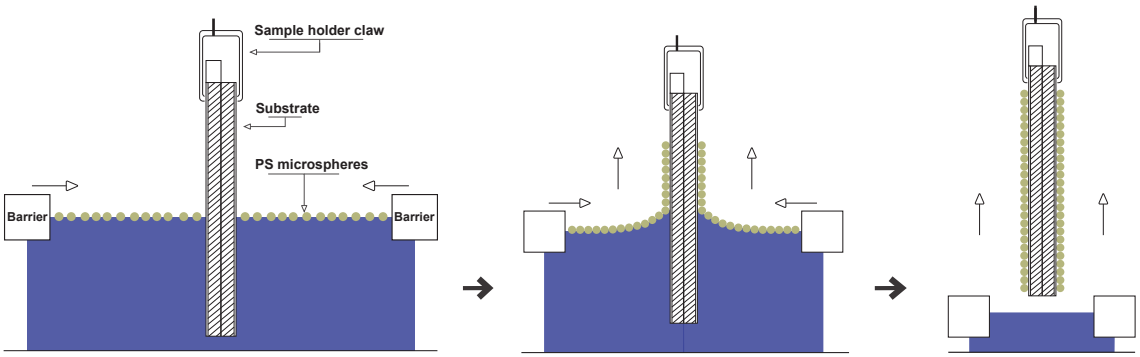

Figure B.1: Schematic of LB process.

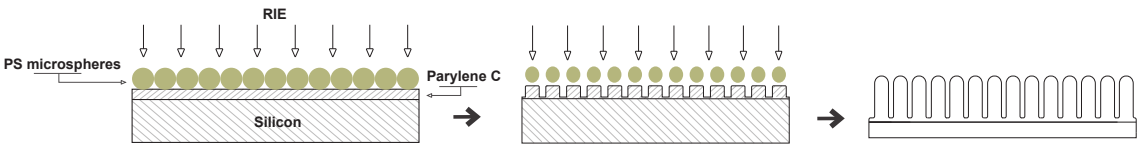

Figure B.2: Schematic of RIE process.

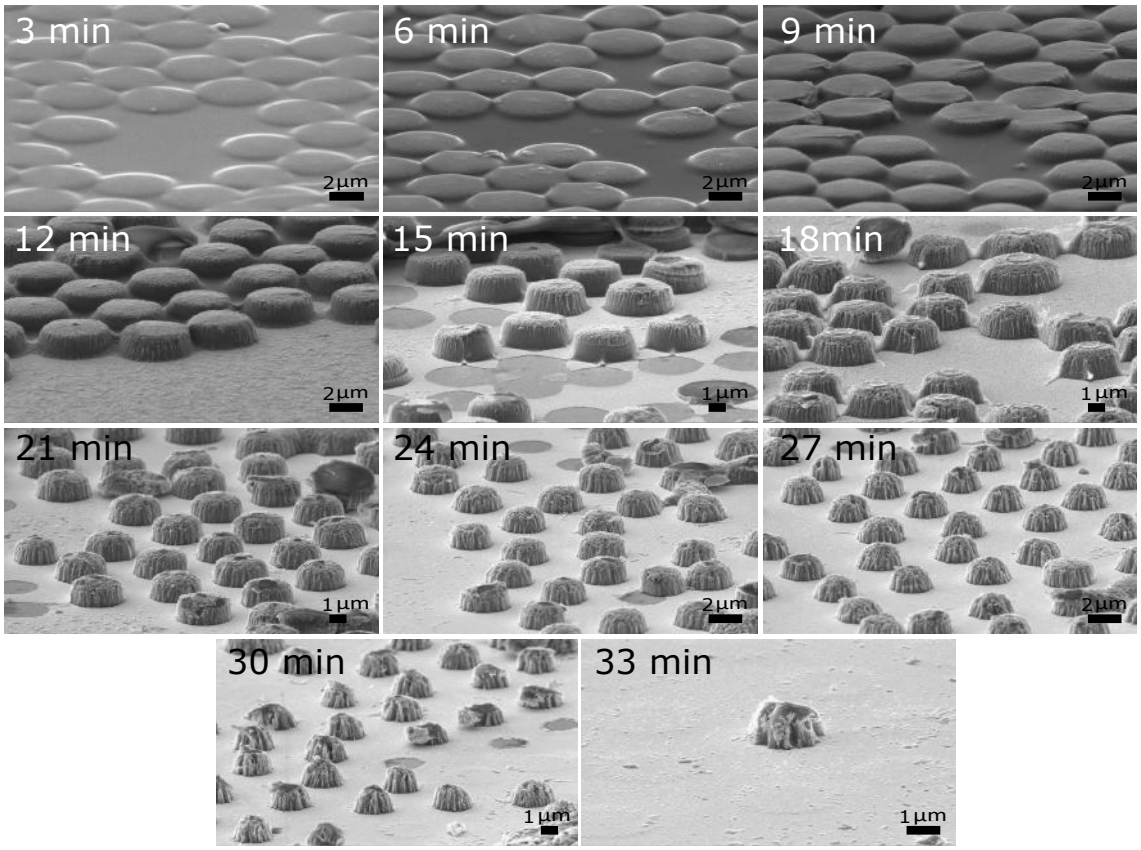

Figure B.3: SEM images of the structures created in Parylene C by the RIE process, with PS spheres as a mask, for several RIE exposure times (45º view).

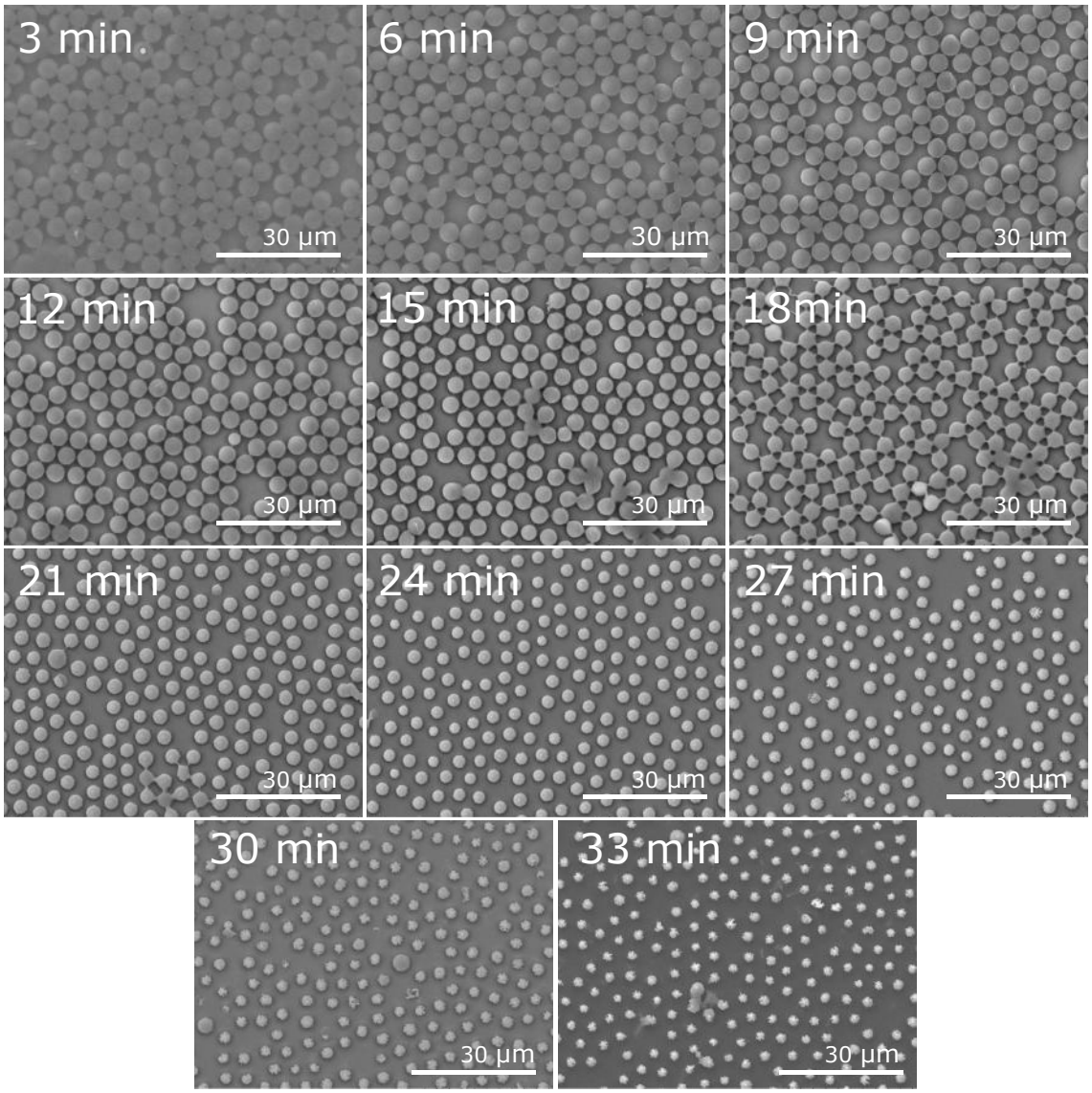

Figure B.4: SEM images resulting from the study of the diameter variation of the structures created in Parylene C by the RIE process, with PS spheres as a mask

Appendix C

This appendix shows the molds used in the production of pyramid-shaped microstructured films as well as the SEM images of microstructured films after peel-off.

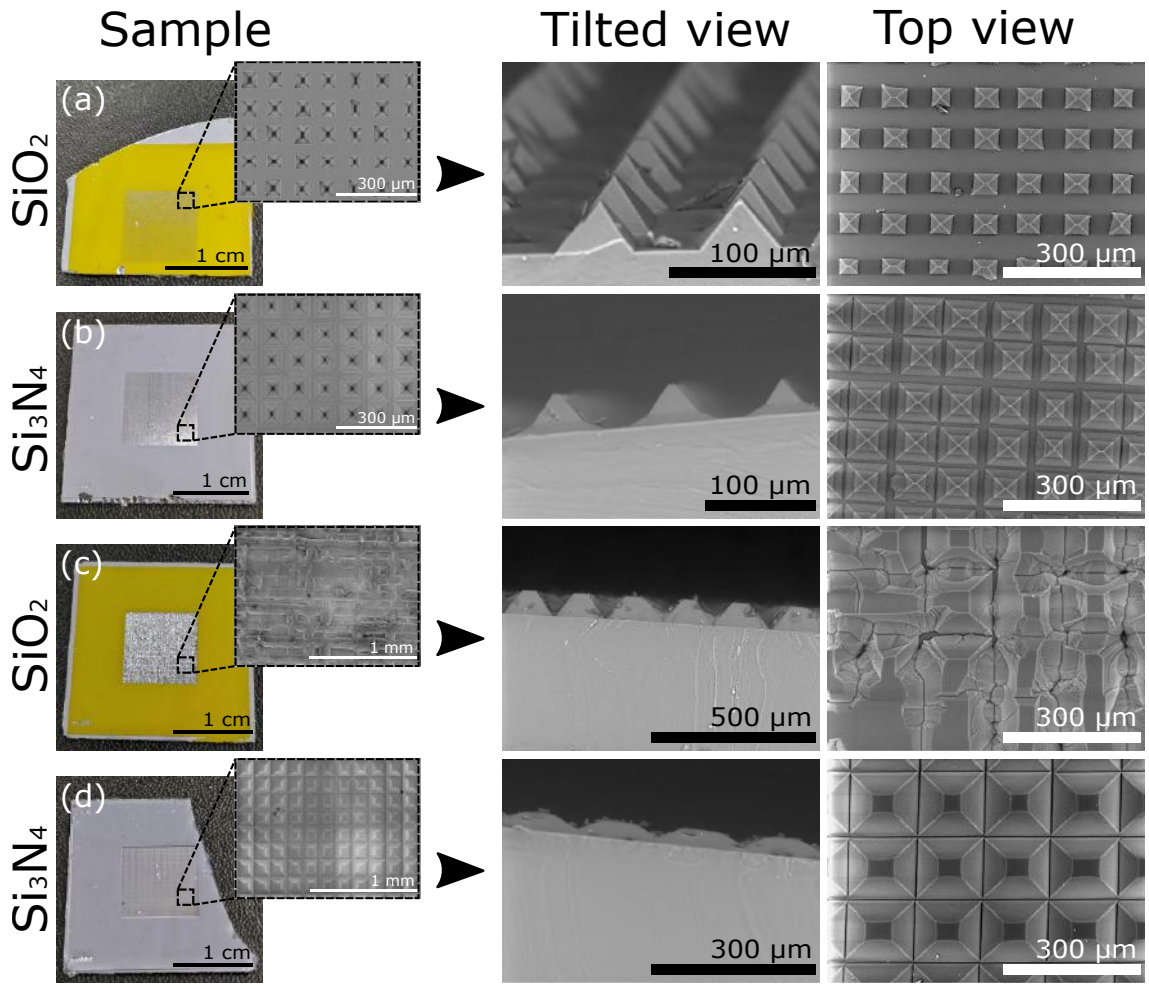

Figure C.1: Photos of pyramid shape silicon molds with SEM image, and SEM images of the respective patterned film after peel-off (tilted and top view): (a) a mold of Si_3N_4 patterned with squares of 50 μm; (b) a mold of SiO_2 patterned with squares of 50 μm; (c) a mold of Si_3N_4 patterned with squares of 100 μm; (d) a mold of SiO_2 patterned with squares of 100 μm.